THESIS

SEX DEPENDENT REGULATION OF IMMUNE RESPONSES IN EX VIVO LUNG SLICES

Submitted by

Brielle Honor Patlin

Department of Biochemistry and Molecular Biology

In partial fulfillment of the requirements

For the Degree of Master of Science

Colorado State University

Fort Collins, Colorado

Spring 2023

Master's Committee:

Advisor: Chris Snow
Co-Advisor: Stuart Tobet

Soham Chanda

ABSTRACT

SEX DEPENDENT REGULATION OF IMMUNE RESPONSES IN EX VIVO LUNG SLICES

Sex differences in respiratory disease have been increasingly obvious over the last several decades ranging from asthma, to interstitial lung disease, to the common cold. One way that lung functions are dependent on sex is in their immune responses to disease. While there are many factors that contribute to the severity of immune responses and recovery from illness, neuroimmune signaling is an understudied aspect. This could be partially caused by the difficulty of studying individual neuronal circuits in the periphery in live animals and the lack of necessary cell types in organoid or cell line models. To study these processes in the lung, an organotypic model, known as a precision cut lung slice (PCLS) can be utilized to maintain intracellular and extracellular signaling. The first study herein addresses the role of the most prevalently produced neuropeptide in the lung on immune, neuronal, and epithelial populations in the lung. This abundant neuropeptide, calcitonin gene related peptide (CGRP), generates several sex dependent responses in PCLS. With CGRP treatment, number of B cells, size of neuroendocrine bodies (NEB), and surfactant protein C (SPC) granule are higher in female PCLS. However, the number of CGRP immunoreactive fibers in female PCLS is lower than in male PCLS. These sex related changes of lung cell behavior may partially explain some disease susceptibilities and are important factors to consider in pharmaceutical development for respiratory diseases.

PCLS can be used to test pharmaceutically relevant substances and drug delivery systems. The recent pandemic has made it evident that better ways to deliver pharmaceuticals to the lungs are required. Regarding this problem, a focus on nasal drug delivery is important. The current leading technology in this type of delivery mechanism involves utilizing lipid nanoparticles and nasal administration. However, this is not the most efficient way to treat the lungs. Crystallized protein structures have begun to be used for purposes other than determining protein structure. In the second study included here, protein crystals were loaded with biologically relevant molecules to purposefully induce immune responses, without causing an immune response by themselves. This functionality has a variety of benefits, because a primary problem in respiratory disease is over activation of the immune response. In this study, crystals were customized by loading different molecules (e.g., lipopolysaccharide (LPS)) and the immune modulatory affects were observable in PCLS. This generated a sex dependent immune response in PCLS, which was less over time than slices treated with pure LPS indicating a differential response over 48 hours. Using protein nanocrystals for pharmaceuticals may provide new ways to target respiratory disease by nasal delivery with benefits over lipid nanoparticles.

TABLE OF CONTENTS

Chapter One/Introduction

Precision cut lung slices (PCLS) are organotypic lung slices that can be used for ex vivo experiments. PCLS have been used over the last several decades to study everything from metabolite expression to drug effects. Although the idea of lung slices was first explored in the early 40s, slices at that time lasted only a few hours. It wasn't until the late 80s when the model started to develop into its current form, no longer being sliced by hand and containing an airway inflation step, that it became used for long term translational studies outside of an animal and maintained structural characteristics (Liu et al. 2019; Alsafadi et al. 2020). Studying the lung in slices has a variety of advantages. First, they contain a variety of cells that can maintain their intercellular signaling. Because of this localization which mirrors what would be seen in vivo, a larger variety of signaling pathways and cellular crosstalk can be studied. Second, extra-organ signaling is eliminated, and lung circuits and metabolism can be explored without complicated hormonal and central nervous system signals. They further provide a way to visualize and treat conditions that are induced by in vivo models. Animals can be exposed to stress or disease conditions and small animal models such as mice can be genetically engineered to reflect a variety of traits from production of fluorescence in specific cells to being germ free (Vandamme 2014). Those animals can then be used to generate slices and many parallel experiments can be performed to look at time or treatments as variables. Slices also have been shown to maintain a variety of physiologically expected behaviors such as movement of the mucociliary ladder and airway contraction in response to various stimuli (vom Steeg et

al. 2020; Cadieux et al. 1999; Held, Martin, and Uhlig 1999; Li, Cohen, et al. 2020; Lam, Lamanna, and Bourke 2019). Most recently, PCLS are starting to be used for translational medicine and drug testing studies (Kapalczynska et al. 2018; Newman 2017; Enlo-Scott et al. 2021; Regal and Johnson 1983; Van Norman 2019; Viana, O'Kane, and Schroeder 2022; Uhl et al. 2015; Freeman and O'Neil 1984; Liu et al. 2019). These studies represent a way to test novel drugs and drug delivery mechanisms in more complete environments than dissociated cell culture models and without the risks of live animal testing (Benam, Konigshoff, and Eickelberg 2018; Vandamme 2014; Jimenez-Valdes et al. 2020). Another potential use would be the use of precision cut lung slices from tissue explants for disease diagnostic or pandemic screening (Dragunas et al. 2020; Burgstaller et al. 2021; Kiener et al. 2021; Lyons-Cohen et al. 2017).

While any kind of lung tissue slices tend to be referred to as precision cut lung slices, the preps and results are diverse. For example, some preps create decellularized structures and others are generated from lung tissue explants (Burgstaller et al. 2021; Leiby et al. 2022; Rosmark et al. 2022; Levesque, Vosatka, and Nielsen 2000; Ruigrok et al. 2019). The types of cells maintained in each prep are different, especially if the cells are introduced in a seeding procedure. However, for clinical relevance, the maximum number of cell types and interactions need to be maintained.

There are a variety of factors to consider when designing and optimizing a precision cut lung slice model. For example, reinflation of the lung after the thoracic cavity is opened, time before the slice is in culture, and the composition of the media. In PCLS preps, the lungs can be reinflated with a variety of substances including agarose,

agar, or media (Alsafadi et al. 2020). The agarose and the agar are used at a variety of different concentrations. A lower concentration will be a less dense polymer and may not provide a sufficiently rigid structure necessary to generate slices. By comparison, too high a concentration of agarose may be difficult to work with, because it will polymerize too quickly, and at high concentrations, damage the morphology (Leiby et al. 2022; Gerpe et al. 2018; Bailey et al. 2020). Inflation with media provides a different challenge because it does not provide any additional rigidity for lung structure. For this reason, these lungs are often frozen before slicing which can also damage the lung. It is important to inflate with a low-density polymer that will provide enough necessary structural rigidity for slicing. Because of the differences in inflation and different strategies to slice the lungs, there is also a variation in the time between when the animal dies and the slices are in culture. Some preps call for the lungs to be left on ice for twenty minutes, some require the lung to be frozen for varying lengths of time, and others simply submerge the lung in a cold solution (Sauer et al. 2014; Benam, Konigshoff, and Eickelberg 2018; Preuss et al. 2022; Patel et al. 2021). Ultimately, the speed of the procedure correlates with the health of the tissue, meaning that a faster method will result in a longer lasting and healthier PCLS. Another factor which contributes to the viability of a PCLS model for translationally relevant research is the composition of the culture medium. For example, the glucose concentration is highly relevant to disease, physiological glucose is 4mM-5.5mM comparatively 7.8mM glucose is considered high blood sugar and 11 is diabetic. Most preps, regardless of type, utilize DMEM/F12 media (11320-Thermo Fisher Scientific) which has a 17.5mM glucose content. Another commonly used media: medium 199 (11150- Thermo Fisher Scientific)

has a 11mM glucose level and a comparatively rarely used media RPMI 1640 (11875-Thermo Fisher Scientific) is one of the only medias to have a relatively normal physiological glucose content at 5.5 (Patel et al. 2021). Another factor to consider when choosing a media is whether it contains or requires the addition of serum. Fetal bovine serum is commonly used, but contains a variety of antibodies, proteins, and growth factors, all of which could introduce variability into an experiment. It is also difficult to repeat, because it is generated from an animal, and each batch will have different components and different concentrations of the components (Gstraunthaler, Lindl, and van der Valk 2013; Stout et al. 2022; Usta et al. 2014; Gurdal et al. 2018). Many PCLS prep medias also include antibiotics, while this may prevent infections, it is important to note that the lungs contain a significant microbiome that is integral for health. The microbiome is also highly relevant in a variety of lung diseases such as cystic fibrosis and chronic obstructive pulmonary disease (COPD). For these reasons, including antibiotics in media makes it less clinically relevant (Schwerdtfeger et al. 2019). Finally, for any study which considers sex as a biological variable, it is important to omit phenol red. Phenol red is a pH indicator which is often included in commercial media and acts as an indicator for health and infection via color change. However, phenol red contains a contaminant that is estrogenic, and therefore can change physiological features of interest (Bindal et al. 1988; Brill et al. 2015; Inam et al. 2022).

The type of model and how it is designed is important to study respiratory diseases and often varies for this purpose. Because of the customizable nature of PCLS, they are highly useful for respiratory disease studies that aim to answer questions about disease pathways, disease progression, therapies, and even

diagnostics. Respiratory disease kills millions of people every year(Niemeyer et al. 2018; McNicholas et al. 2019; Jin et al. 2020; Mathers, Boerma, and Ma Fat 2009; Li, Cao, et al. 2020). By itself, COPD is the third leading cause of death in the world, and many respiratory disease therapies are not wholly effective. In the extreme cases where lung transplant is called for, 50% of patients die within six years (Thabut and Mal 2017; Foroutan et al. 2019; Rello et al. 2017). Despite the research efforts which are being put toward respiratory diseases there are a variety of aspects that are not routinely explored because of the broad scope of these illnesses. A disease can affect the microbiome, neural populations, immune populations, oxygen transfer, mucus production, and more and they tend to be different based on the sex and age of the individual which makes it difficult to fully encompass all aspects of a disease when studying it (Trigueros et al. 2019; Barnes 2016; Hong et al. 2016; Bai et al. 2022; Sauler, Bazan, and Lee 2019; Ruigrok et al. 2019; Noguchi, Furukawa, and Morimoto 2020).

Sex differences in immune responses and mortality to respiratory diseases are found across species (Klein and Flanagan 2016). Respiratory inflammatory diseases are more common in females compared to males and males are more susceptible to diseases such as COVID-19 and pneumonia (Klein, Bird, and Glass 2001; Chamekh et al. 2017). Patients presenting with similar symptoms of the same age and fitness can have drastically different outcomes according to sex (Trigueros et al. 2019; McNicholas et al. 2019; Kautzky-Willer et al. 2022; Ursin and Klein 2021; Hong et al. 2016; Tejpal et al. 2021). In the lung, sex dependent neural differences include changes in acetylcholine release and neuromuscular function, regulation of airway constriction, ciliary clearance, and mucus secretion (Han et al. 2018; Carey, Card, Voltz, Germolec,

et al. 2007; Townsend, Miller, and Prakash 2012; LoMauro and Aliverti 2018; Dominelli and Molgat-Seon 2022; Fuseini and Newcomb 2017). These sex differences are influenced by sex steroid hormones, allergen exposure, exercise, and other factors that are difficult to control for using in vivo mice models (Ursin and Klein 2021; Williams 2014; Ying et al. 2022).

Recently, it has become apparent that the role of neuropeptides and neural signaling in the lung are imperative to study respiratory diseases. A key question for the diverse components of disease resistance and progression is the issue of systems integration. It might be obvious to consider roles for neural - immune signaling in the central nervous system, but perhaps less obvious in respiratory disease responses. Neural fibers in the lung contain a variety of neuropeptides including vasoactive intestinal peptide (VIP), calcitonin gene related peptide (CGRP), substance P, and others. CGRP producing fibers are highly prevalent in the lung and are known to have a variety of disease relevant interactions. CGRP is broadly implicated in neuroimmune axis function of the lung. It plays a role in mucus secretion (Atanasova and Reznikov 2018) and has been shown to limit the effects of some inflammatory cytokines (Nagashima et al. 2019). CGRP antagonists are being used to treat migraine (Assas 2021; Deen et al. 2017; Durham 2006; Durham and Vause 2010; Benemei et al. 2009; Ray et al. 2021) and agonist effects are being evaluated in cancer (Ostrovskaya et al. 2019; Dallmayer et al. 2019; Hoppener et al. 1987; Gutierrez and Boada 2018; Zhang et al. 2020). CGRP effects are further implicated in an increasingly wide range of health issues including Alzheimer's disease, vascular health, hypertension, and pregnancy (Rashid and Manghi 2022; Singh et al. 2017; Kee, Kodji, and Brain 2018). Given the

broad variety of roles of CGRP, its agonists and antagonists relevant to the development of therapeutics, it is important to understand the cell – cell signaling pathways of this peptide in lungs.

CGRP is a 37 amino acid peptide that has alpha and beta forms. While the CGRPα and CGRPβ isoforms are nearly identical in structure— differing by only 3 amino acids—they are made from separate genes in different locations. CGRPα is systemic and CGRPβ is localized to the enteric nervous system (Russell et al. 2014). CGRPα is made from a gene splice variant of the gene for calcitonin which is also known as procalcitonin—a peptide which can be used to identify bacterial pathogenesis through blood samples (Mazaheri et al. 2022). The alpha isoform is the most abundant manifestation of the peptide throughout the body (i.e., lungs) and has widespread peripheral effects including vasculature constriction and pain (Russell et al. 2014). Commonly associated with C fibers, this peptide has receptors throughout the body. While normal levels of CGRP are around 1μM in circulation, in the presence of inflammatory factors or capsaicin, CGRP release can be increased to up to 10μM in serum (Durham 2006).

While the neuroimmune aspects of disease in the lung are underexplored, drug targeting to proteins produced by other cell types are frequently studied. There are wide ranging treatments relevant to the lung from systemically presented shots and vaccinations to nasal sprays (Tiwari et al. 2012; Zhang et al. 2022). However, the current methods for drug delivery can be improved upon. Nasal administration of drugs and vaccines has been pervasive lately as a technique to immunize nasal membranes, and also the throat and the lung with rapid immune activation. Current technologies

such as those produced by Pfizer and Moderna rely on lipid nanoparticles as a delivery mechanism. Lipid nanoparticles have several advantages including an adjuvant affect. An aggravation of the immune system may not be ideal in all treatment however, because many respiratory diseases can over activate the immune system leading to death. Lipid nanoparticles can be made to contain an assortment of different biologically relevant molecules and are relatively easy to produce (Xu, Tao, and Wang 2020; Fang et al. 2020). Because they are coated with a high concentration of membrane proteins and lipids, they are absorbed into lipid membranes relatively easily. This allows them to deposit their contents inside cells. However, this property also prevents lyophilized lipid nanoparticles present in a spray from reaching all the way to lung membranes. Some disadvantages of this system are caused by the nature of a lipid nanoparticle. They provide minimal protection to the drugs contained within. Because they are composed of lipids, it is difficult to load hydrophilic molecules. The amount of the drug delivered can be highly variable (Birkhoff, Leitz, and Marx 2009; Grassin-Delyle et al. 2012). Further, application of these nanoparticles may result in a systemic rather than targeted drug delivery (Wu et al. 2021; Xu, Tao, and Wang 2020; Crowe and Hsu 2022). Therefore, a specific delivery mechanism that does not have innate adjuvant properties and is not absorbed into lipid membranes, but still can be loaded with a wide range of biologically relevant molecules may be useful.

One such delivery vehicle has been developed in the Snow lab in the form of loadable protein micro- and nanocrystals. For decades protein crystallization has been used for deducing the structure of proteins, but recently it has been demonstrated that these crystals can be engineered to form porous, loadable, and customizable shells.

Crystals can be grown from CJ, a roughly 19.1 kDa trimeric protein produced in E. coli, that can be reproducibly grown to diameters above 100 μm, and smaller than 500 nm, by altering the batch growth conditions – in particular, total protein concentration, precipitant concentration, and pH (Hartje et al. 2017). These crystals display the unique property of adsorbing nucleic acids with strong binding affinity (Hartje et al. 2018). However, these crystals have not previously been tested for use in drug delivery. Therefore, it would be necessary to test their adjuvant properties, their absorbability into tissue, and their potential to cause inflammatory responses on their own.

In the current studies, the neuroimmune axis of disease and the potential role of protein crystals were utilized to assess a sex related immune response in PCLS that I first show in Chapter 2. In the experiments of Chapter 3, the PCLS model was assessed for health and characterized for a variety of populations including neural fiber populations. To test the immune stimulatory properties of protein crystals, they were introduced to PCLS and compared to tissue not exposed to crystals, and crystals loaded with a purposefully immune stimulating molecule. The role of the most prevalent neuropeptide in the lung was assessed in a sex selective manner resulting in changes to B cells and pulmonary neuroendocrine cells (PNECs).

Chapter Two/Neuropeptides Stimulate Physiological and Immunological responses in Precision Cut Lung Slices[1]

Graphical Summary

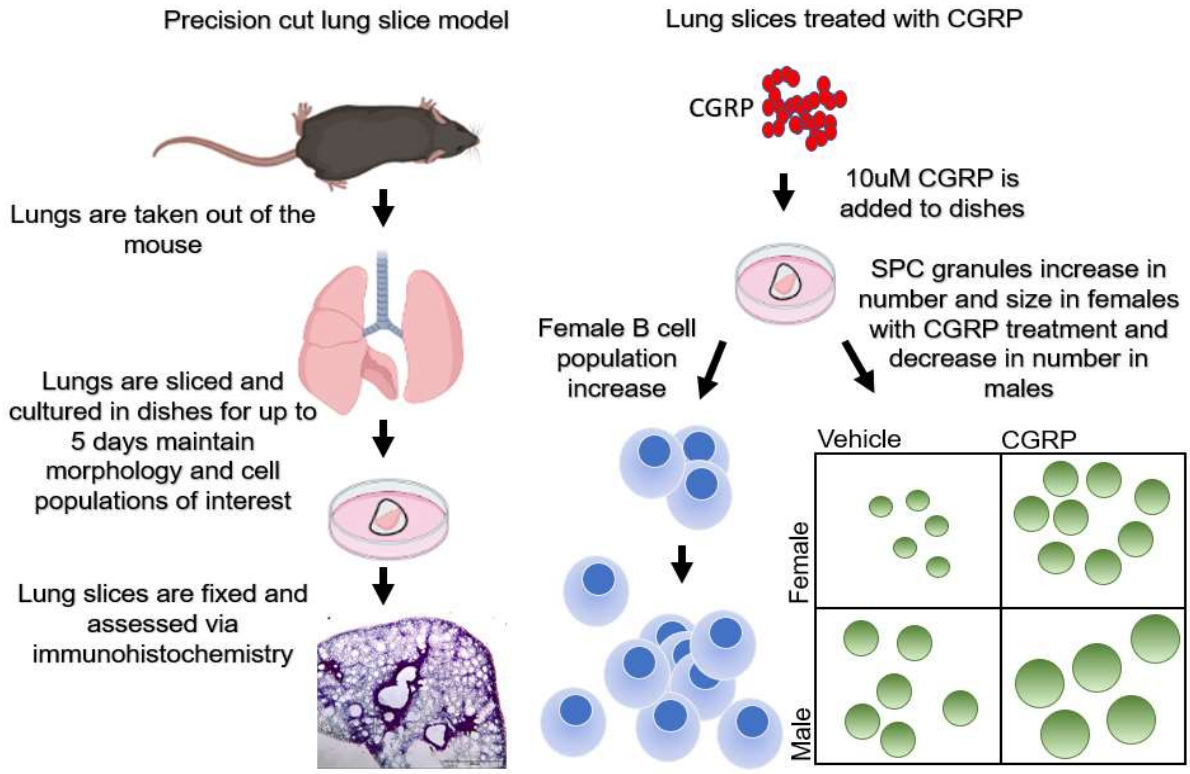

Figure 1: Graphical Summary

[1] B. Patlin[1], L. Schwerdtfeger[2], S. Tobet[3*]

Author information

1. B. Patlin, Department of Biochemistry and Molecular Biology, Colorado State University, Fort Collins, CO.
2. L. Schwerdtfeger, Department of Neurology, Harvard Medical School and Ann Romney Center for Neurologic Diseases, Brigham and Women's Hospital, Boston, MA.
3. S. Tobet, School of Biomedical Engineering and Dept of Biomedical Sciences, Colorado State University, Fort Collins, CO.

Overview

Organotypic lung slices, sometimes known as precision cut lung slices (PCLS) provide an environment in which numerous cell types and interactions can be maintained outside the body (ex vivo). PCLS were maintained ex vivo for up to a week and demonstrated health via the presence of neurons, maintenance of tissue morphology, synthesis of mucopolysaccharides, and minimal cell death. In the current study we characterized lung neuropeptides ex vivo. There were multiple distinct types of neuronal fibers present in lung slices with varied size, caliber, and neurotransmitter immunoreactivity. Of the neuropeptides present in fibers, calcitonin gene related peptide (CGRP) was the most prevalent. Exposing PCLS to recombinant CGRP resulted in proliferation and dispersion of $CD19^+$ B cells in slices only from females. The number of granules containing immunoreactive (ir) surfactant protein C (SPC), which are representative of alveolar type 2 cells (AT2), increased in slices from females within 24 h of exposure to CGRP. Additionally, ir-SPC granule size increased in slices from females across 48 h of exposure to CGRP. Treatment of PCLS with CGRP resulted in a stable pulmonary neuroendocrine cell (PNEC) population and increased neuroendocrine body (NEB) size. While no changes in total fibers were observed based on ir-peripherin, ir-CGRP in fibers was absent in fibers, but retained in PNECs. These changes provide insight to innate immune and neuroendocrine responses in lungs that may be partially regulated by neural fibers. The sex dependent nature of these changes may point towards an explanation for sex selective outcomes for respiratory diseases.

Introduction

The lungs are a primary surface of interaction with the external world—encountering pathogens, dirt, yeast, smoke, and other particulates in the thousands of liters of air an average person breathes every day (Valavanidis et al. 2013; Fang et al. 2020). These particulates can cause respiratory damage, leading to pathology including chronic obstructive pulmonary disease (COPD). Respiratory diseases like COPD are highly sex-dependent (Trigueros et al. 2019; Barnes 2016; Hong et al. 2016)and cause nearly four million deaths globally every year (Li, Cao, et al. 2020). While significant research efforts are devoted to studying the etiology of these diseases and pathways towards treatments, many unanswered questions about the nature of respiratory disease progression remain to be explored (Li, Cao, et al. 2020). Investigations of the diverse components of respiratory disease resistance and progression require methods that consider systems integration to account for myriad cell-cell interactions involved in disease etiology. In particular, the role of neural immune signaling (i.e., neuroimmune) at a local level requires further derivation. This study utilizes precision cut lung slices (PCLS) that maintain neural and immune elements inside the lungs, allowing investigation of complex neuroimmune signaling pathways (Blake, Jiang, and Chiu 2019).

A variety of cells in the lung produce neuroactive peptides such as calcitonin gene related peptide (CGRP), vasoactive intestinal peptide (VIP), and substance P. These neuropeptides regulate functions in the lung such as cell proliferation, nociception, and controlling airway homeostasis (Dakhama, Larsen, and Gelfand 2004; Assas, Pennock, and Miyan 2014). CGRP is broadly implicated in neuroimmune axis

functions of the lung. It plays a role in mucus secretion (Atanasova and Reznikov 2018) and has been shown to limit the effects of some inflammatory cytokines (Nagashima et al. 2019). CGRP antagonists are being used to treat migraine (Assas 2021; Deen et al. 2017; Durham 2006; Durham and Vause 2010; Benemei et al. 2009; Ray et al. 2021) and agonist effects are being evaluated in cancer (Ostrovskaya et al. 2019; Dallmayer et al. 2019; Hoppener et al. 1987; Gutierrez and Boada 2018; Zhang et al. 2020). CGRP driven responses are further implicated in an increasingly wide range of health issues including Alzheimer's disease, vascular health, hypertension, and in pregnancy (Rashid and Manghi 2022; Singh et al. 2017; Kee, Kodji, and Brain 2018). Given the broad roles of CGRP in homeostasis and disease, it is important to understand the cell signaling pathways of this peptide in lungs.

CGRP is a 37 amino acid peptide with alpha and beta forms. While CGRPα and CGRPβ isoforms are nearly identical in structure— differing by only 3 amino acids— they are coded by separate genes. CGRPα is systemic while CGRPβ is localized to the enteric nervous system (Russell et al. 2014). CGRPα is made from a gene splice variant of the gene for calcitonin which is also known as procalcitonin—a peptide which can be used to identify bacterial pathogenesis through blood samples (Mazaheri et al. 2022). The alpha isoform is the most abundant manifestation of the peptide throughout the body (i.e., lungs) and has widespread peripheral effects including vasculature constriction and involvement in pain (Russell et al. 2014). Commonly associated with C fibers, this peptide has receptors throughout the body. While normal levels of CGRP are around 1μM in circulation, in the presence of inflammatory factors or capsaicin, CGRP release can be increased to up to 10μM in serum (Durham 2006).

Pulmonary neuroendocrine cells (PNECs) are a cell type in the lungs that produce CGRP and express CGRP receptors. These specialized epithelial cells are innervated by CGRP immunoreactive neuronal fibers and contain neuropeptides, amine hormones, and peptide hormones (Cutz 1982). PNECs cluster and are referred to as neuroendocrine bodies (NEBs). PNECs and NEBs are commonly located near the intersection points of airways and vasculature (Sui et al. 2018) that regularly also contain germinal centers with a variety of resident immune cells including B cells. PNEC behaviors have been incompletely characterized and are different when cells are isolated vs. in clusters (Noguchi, Furukawa, and Morimoto 2020). Solitary PNECs are located sporadically throughout the airway epithelia and move in response to stimulation. Conversely, NEBs are usually located near airway junctions and do not move. NEBs have been theorized as a type of progenitor cell population which can become cancerous in lung with specific mutations (Wallrapp et al. 2019; Gutierrez and Boada 2018; Noguchi, Furukawa, and Morimoto 2020). PNECs and NEBs have been suggested to act as chemo sensors (Gu et al. 2014). Although these cells are reportedly rare, there are several factors which stimulate population expansion or an increase in cell size (Mou et al. 2021) including hypoxia, lung injury, and disease (Shivaraju et al. 2021).

Sex differences in immune responses and mortality to respiratory diseases are found across species (Klein and Flanagan 2016). Respiratory inflammatory diseases are more common in females compared to males; however, males are more susceptible to diseases such as COVID-19 and pneumonia (Klein, Bird, and Glass 2001; Chamekh et al. 2017). Patients presenting with similar symptoms of the same age and fitness can

have drastically different outcomes depending upon their sex (Trigueros et al. 2019; McNicholas et al. 2019; Kautzky-Willer et al. 2022; Ursin and Klein 2021; Hong et al. 2016; Tejpal et al. 2021). In the lung, sex dependent neural differences include changes in acetylcholine release and neuromuscular function, regulation of airway constriction, ciliary clearance, and mucus secretion (Han et al. 2018; Carey, Card, Voltz, Germolec, et al. 2007; Townsend, Miller, and Prakash 2012; LoMauro and Aliverti 2018; Dominelli and Molgat-Seon 2022; Fuseini and Newcomb 2017). These sex differences are influenced by sex steroid hormones, allergen exposure, exercise, and other factors that are difficult to control for using in vivo mice models (Ursin and Klein 2021; Williams 2014; Ying et al. 2022).

To study lung functions with good control of environmental variables, an organotypic lung slice model (PCLS) was optimized for tissue maintenance ex vivo for up to a week. Few studies use PCLS models to study neural influence over lung physiology, and studies that do mostly consider airway smooth muscle regulation by respiratory neural components but not immune cells (Schleputz et al. 2012; Kummer et al. 2006; Bai et al. 2022; Lam, Lamanna, and Bourke 2019; van den Berg et al. 2021). Studies that have examined the roles of neuropeptides have either utilized electric field stimulation or explored the role of substance P in relation to MUC5AC expression and airway contraction (Springer and Fischer 2003; Sponchiado et al. 2021; Voedisch et al. 2012; Regal and Johnson 1983). Ex vivo models allow for direct introduction of stimuli and observation of anatomically localized responses. In the current study, lung specific interactions relevant to the neuroimmune axis were examined, in PCLS to investigate CGRP effects on alveolar type two (AT2) cells, $CD19^{+}$ B cells, PNEC/NEB, and

neuronal fiber populations.

Materials and Methods

Animals: Young adult male and female C57BL/6J mice transgenic for YFP expressed on the Thy-1 promoter (JAX:003709) were used for all experiments (Tobet et al. 2003; Feng et al. 2000). Animals were housed in the Painter Center building and were cared for by Laboratory Animal Resources at Colorado State University. Cages were supplied with aspen bedding (autoclaved Sani-chips; Harlan Teklad), tissues for nesting, and red igloo mouse houses. Mice were exposed to a 14:10 h light-dark cycle and had access to water and food ad libitum (no. 8640; Harlan Teklad). Animals were cared for and utilized according to the Colorado State University IACUC protocol #1934.

Generation of PCLS: Adult mice were anesthetized using isoflurane and killed via cervical dislocation. The thoracic cavity was opened by cutting through both sides of the ribs and then severing the diaphragm across the midline. Animals were perfused through the heart with 37˚C phosphate buffered saline (PBS) for quantitative analyses or PBS containing 0.1mg / ml FITC to aid visualization of the vasculature for qualitative examination and imaging. Hearts were removed and the thymus and salivary glands were dissected away under an Olympus SZX7 dissecting scope until the trachea was clearly visible. The trachea was partially perforated so that a 20-gauge needle could be inserted. The lungs were inflated using 1 ml of 40°C 2% low melting point agarose (Gold Biotechnology, St. Louis, MO) in MQH_2O until the lung was visibly inflated to the edge of the lobe without rupturing. Lungs were removed and immediately placed in ice cold Krebs. Using the Olympus SZX7 dissecting scope trachea and blood clots were dissected from the exterior of the lung and lobes were separated. Single lobes of the

lung were then placed in ~40°C 8% low melting point agarose in MQH_2O at 4°C for 4 minutes to permit the agarose to polymerize and enable cutting of 250μm thick slices using a vibrating microtome (VT1000S; Leica Microsystems, Wetzlar, Germany). Slices were collected into 5 ml hibernate media (Life Technologies, Grand Island, NY) in 60mm dishes (Corning, Corning, NY) at 4°C for at least 15 minutes; hibernate was then removed and replaced with 5 ml of adult neurobasal culture media (ANB; Life Technologies) with 2% B27 supplement (Life Technologies) for 35 minutes at 37°C to permit slices to regain physiological temperature. This media was serum free to increase the reproducibility of experiments (Schwerdtfeger et al. 2019) and antibiotics were omitted from the media to promote maintenance of lung microbiota and translational relevance. Slices were relocated to 35mm plastic bottom culture dishes (Corning and Corning Falcon, Corning, NY) sans media for 15 minutes at 37°C and 100% humidity to promote adherence to the dish. Slices were then covered with a thin layer of collagen solution (vol/vol: 10.4% 10× MEM, 1.9% PS, 4.2% sodium bicarbonate, and 83.5% collagen (PureCol; Inamed, Fremond, CA)) for 10 minutes at 37°C before 0.8 ml of adult neurobasal media with 2% B27 supplement was added to each dish to create a culture with an air liquid interface. Media was changed daily throughout the culture period.

Neuropeptide treatment: PCLS were treated with 10μM CGRPα peptide (015-09; Phoenix Pharmaceuticals) for 24-, or 48 h. Dosage was based on levels of CGRP released from trigeminal neurons in response to different stimuli (Durham 2006). To confirm dosage, slices were treated with 1μM or 10μM and compared for B cell response. 10μM CGRP addition generated a larger B cell response and thus was used

for all experiments. At the end of the incubation/treatment period, slices were fixed in 4% paraformaldehyde for 15 minutes and washed 3x for 1-2min with PBS.

Biochemical Analyses: Cell death was visualized by incubating live slices for 10 minutes using acridine orange (A1301; Invitrogen, Thermo Fisher Scientific) at 1µl per 0.8 ml media (2µM) followed by 3x 30-minute washes with 1 ml of media (Byvaltsev et al. 2019). In live tissue slices, acridine orange can be used to visualize a variety of different structures when excited with either blue light or green light. When excited with blue light all cells will be visible as the compound binds to cytoplasmic RNA. When excited with green light, only cells with permeable nuclei will be visible due to DNA binding. These fluorescent emission patterns are significantly different than when acridine orange is used on fixed tissue and does not require the use of propidium iodide (Byvaltsev et al. 2019). Tissue health was confirmed by live treatment and imaging of tissue slices treated with acridine orange. All cells were visualized by acridine orange binding to RNA using a fluorescein/GFP filter set (fluorescent emission 533) and cells with permeable nuclei were visualized by acridine orange binding to DNA using a Texas Red filter set (fluorescent emission 656). Less than 10% of cells visualized had permeable nuclei (data not shown) which become permeable when undergoing division or apoptosis thereby allowing access of acridine orange to DNA. Slices were imaged live using a Nikon TE2000-U inverted. Slices were then fixed for 15 minutes at room temperature with 2 ml 4% paraformaldehyde per 35mm dish. Ethidium homodimer (EtHD; Biotium, Hayward, CA) was also attempted for identification of permeable cells, but EtHD became stuck throughout lung tissue indicating unreliable fluorescence. To assess mucopolysaccharide synthesis in lung epithelia, slices were treated with tetraacetylated-

N-Azidoacetylgalactosamine (GalNAz; C33365, Thermo Fisher)) after 0, 24, or 48 h of culture and incubated for an additional 24 h after addition of GalNAz. Slices were fixed using 4% paraformaldehyde and reacted with the fluorophore-tagged alkyne, Dibenzocyclooctyne-Cy3 (DBCO-Cy3; 2 μM; Sigma- Aldrich, St. Louis, MO) to produce fluorescence (Schwerdtfeger, Ryan, and Tobet 2016). To assess cell proliferation, slices were treated with 4μl of 10μM 5-ethynyl-2'-deoxyuridine (EdU; Invitrogen, Eugene, OR) per 0.8 ml of media after 24 h of culture. At 48 h, EdU containing media was removed from slices before fixation with 4% paraformaldehyde. Slices were then washed in PBS for 30 min, followed by 30 min in glycine (Fisher Scientific, Pittsburgh, PA), and 3 more PBS washes to remove any unreacted 4% paraformaldehyde. Slices were blocked in 3% bovine serum albumin buffer (BSA; Lampire Biological, Pipersville, PA) and 0.5% Triton X-100 (Tx; 42235-5000, ACROS) for 2 h, followed by two washes with a 3% BSA solution for 10 minutes each. A click-IT reaction was then performed on the slices using click-IT cocktail (click-IT Reaction Buffer, CuSO4, Alexa-Fluor azide, reaction buffer additive; Invitrogen) for 2 h. Slices were further washed three times in 3% BSA buffer and 0.02% Tx for 30 min each and left overnight in 3% BSA solution. Samples were then mounted on slides and cover slipped for fluorescent imaging by confocal microscopy (Schwerdtfeger, Ryan, and Tobet 2016).

Immunohistochemical Analyses: Slices were fixed for 15 minutes in 4% paraformaldehyde at room temperature and then washed in 0.5M PBS (pH 7.4) prior to whole-mount immunohistochemistry (250μm thick). Slices were incubated at 4°C in 1% sodium borohydride for 2 h. They were then washed in PBS for 10 minutes prior to incubation in a blocking solution comprised of PBS with 5% normal goat serum (NGS;

Lampire Biological, Pipersville, PA), 3% hydrogen peroxide and 0.3% Tx for 2 h with a change of solution at 1 h. Slices were then incubated in primary antisera (see Table 1)

Table 1: Antibodies used for immunohistochemistry

Primary Antibodies	RRID	Source	Secondary Antibodies	RRID	Source	Marker for:
CD19	AB_467151	14-0199-82 eBioscience	Cy3 anti-rat 1:500	AB_2338253	112-166-003 Jackson ImmunoResearch	B-cells
CD79	AB_962641	NB100-64347 Novus Biologicals	Cy3 anti-rabbit 1:500	AB_2338008	111-166-045 Jackson ImmunoResearch	B-cells
Peripherin	AB_90725	Ab1530 Arc Bio	Cy3 anti-rabbit 1:500	AB_2338008	111-166-045 Jackson ImmunoResearch	Type 3 intermediate filament protein
SPC	AB_91588	Ab3786 EMD Millipore	Cy3 anti-rabbit 1:500	AB_2338008	111-166-045 Jackson ImmunoResearch	Surfactant protein C (SPC)
VIP	AB_572270	20077 Immunostar	Cy3 anti-rabbit 1:500	AB_2338008	111-166-045 Jackson ImmunoResearch	Vasoactive intestinal peptide
CGRP	AB_572217	24112 Immunostar	Cy3 anti-rabbit 1:500	AB_2338008	111-166-045 Jackson ImmunoResearch	Calcitonin gene related peptide (CGRP)
ChAT	AB_1968484	NBP1-30052 Novus Biologicals	Cy3 anti-goat 1:500	AB_2340880	805-165-180 Jackson ImmunoResearch	Choline acetyl transferase
Substance P	AB_572266	20064 Immunostar	Cy3 anti-rabbit 1:500	AB_2338008	111-166-045 Jackson ImmunoResearch	Substance P peptide

solution containing 5% NGS, 0.3% Tx, and primary antibodies at various concentrations for 5 days. After sitting in primary antisera solution for 5 days, slices were washed at 4°C in a 1% NGS, 0.2% Tx, PBS solution four times for 30 minutes per wash. Slices were then incubated for 24 h at 4°C in fluorescent conjugated secondary antisera. After 24 h, samples were washed four times for 30 min each in a 0.02% Tx PBS solution before being mounted on slides and cover-slipped with Aqua-Poly/Mount (Polysciences, Warrington, PA).

Microscopy and Image Analysis: Slices were imaged by confocal microscopy using a

Zeiss LSM 880 confocal microscope with an Axiocam 503 mono camera (Carl Zeiss, Inc., Thornton, NY) after fixation or a Nikon TE2000-U inverted microscope for live brightfield or epifluorescence imaging. TE2000-U images were taken using a 20x Plan-Apo objective lens. Live imaging occurred at 37°C with approximately 5% CO2 and atmospheric oxygen conditions using Metamorph Microscopy Automation and Image software. Tissue that was used for live imaging was not processed for other experimental values. For each set of treatment groups (24 h CGRP treated, 48 h CGRP treated, 24 h vehicle treated, 72 h vehicle treated, and 120 h vehicle treated) samples were collected at the same time under the same conditions. Confocal imaging was performed for immunohistochemical analysis of all slices. Imaging occurred after slices were mounted on slides and cover-slipped using Aqua-Poly/mount. At least 3 mice were used for each experiment to account for biological variability. Single plane confocal images were taken using 20x and 40x objective lenses (Plan-fluor). At least one PCLS was analyzed in each analysis. All images were selected to contain the maximal number of puncta of interest with 0 overlap in sets of 12 images. Analysis was considered per slice and n values were reported as the number of slices analyzed. Live imaging was performed for GalNAz, acridine orange, and slices from FITC perfused lungs. Fixation eliminated fluorescence generated by the Thy-1-promoter driving YFP. The investigator conducting all quantitative analyses was blinded to treatment group.

Quantitative Analyses: Analyses were performed for number and/or size of each labeled entity using NIH Fiji (v.2.9.0). The area of immunoreactive SPC was calculated in a series of 12 regions of interest (ROI, 2048-2048-pixel) from single plane images for each experimental value. Neuronal fibers (CGRP-ir and Peripherin-ir) were counted by

area per ROI (2048-2048-pixel) and by area of fibers per slice. Fiber ROI were localized to bronchioles, as bronchioles were the primary site of innervation and 12 ROIs per slice were assessed per experimental data point. CGRP-ir cells (PNECs and NEBs) were counted manually without computer assistance. They were identified in sets of 12 ROIs in single plane images (2048-2048-pixels) from each slice for each experimental value. $CD19^+$ labeled cells were analyzed in 12 ROIs (2048-2048-pixel) selected for by presence of $CD19^+$ cells for each experimental slice data point. All measurements except those for PNECs and NEBs recorded included cell counts, area, mean, and standard deviation.

Statistics: Statistical Analysis was performed using Prism 9.4.0 (graph pad) and Excel software. Two-way ANOVA (sex x time of CGRP) were performed for males vs. females for 24 h CGRP, 48 h CGRP, 24 h vehicle, 72 h vehicle, and 120 h vehicle groups for all analyses. SPCs or $CD19^+$ B cells were quantified by size and number, and CGRP or peripherin by total fiber area and fiber area/slice. Post-hoc testing used a multiple comparison Fisher's LSD test, and all data is presented as mean +/- standard deviation. $P < 0.05$ was considered significant and was represented with one symbol, $P < 0.01$ was represented with two symbols, and $P < 0.001$ was represented with three symbols.

Tissue health/criteria for data inclusion: Only data generated from healthy tissue was utilized in this study. The health of lung slices—maintained ex vivo for five days—was demonstrated using a variety of methods during the optimization process before experiments were performed (supplemental figures S3-S8). Cells lining the bronchioles continued to synthesize mucopolysaccharides ex vivo similar to in vivo (Figure S1). GalNaz Click-chemistry allowed for visualization of newly incorporated mucin-type O-

linked glycoproteins around bronchioles. Ciliary beating was confirmed in slices by visual observation (data not shown). Lung slices (250μm) maintained structural morphology for at least 5 days ex vivo as shown in representative fluorescent images (Figure S2) and using the histological stains, thionin and aldehyde fuchsin (data not shown).

Neuronal fiber integrity was also used as an indicator of health. Such fibers were revealed based on the immunohistochemical detection of peripherin- (Figure S3a), choline acetyl transferase- (Figure S3b), substance P- (Figure S3c), vasoactive intestinal peptide- (Figure S3d), and CGRP-ir (Figure S3e) fiber populations. CGRP-ir fibers had the highest abundance excluding peripherin which is a comprehensive marker for peripheral fibers.

Results

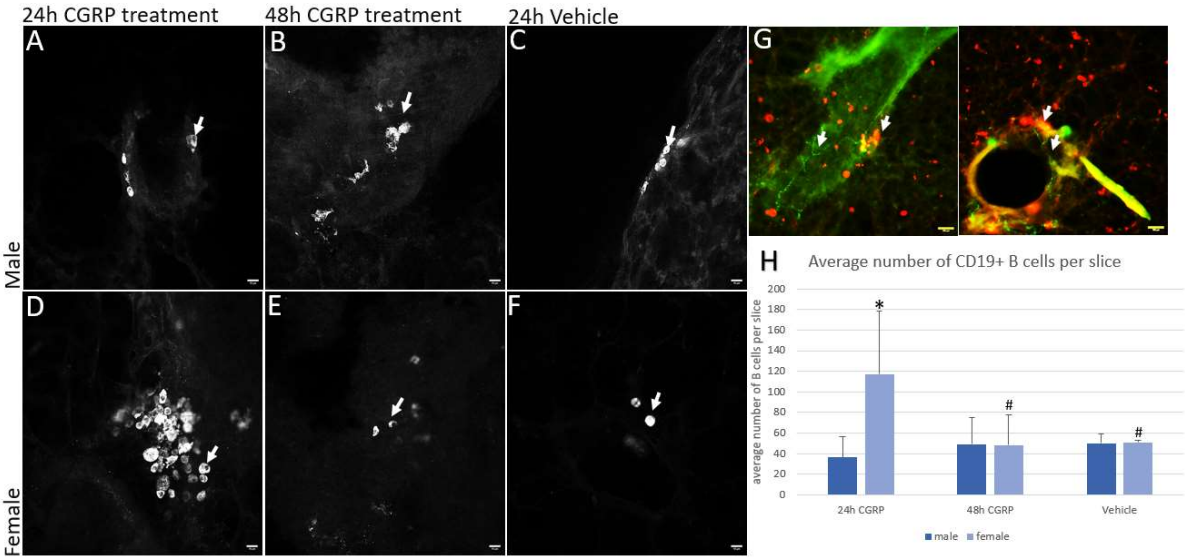

Figure 2: The number of CD19 immunoreactive B cells increased in slices from females but not males upon treatment with calcitonin gene related peptide (CGRP). * Indicates significance between males and females. # Indicates significance compared to 24 h of the same sex. A-C. female PCLS treated with CGRP for 24 or 48 h compared to vehicle. D-F. female PCLS treated with CGRP for 24 or 48 h compared to vehicle. G) CGRP fibers (green) colocalized with B cells (red). H) B cells are highly increased in females at 24 h treatment with CGRP compared to vehicle and much greater than B cells in slices from males. No change was seen at 48 h compared to vehicle or between male and female at 48 h or vehicle. B cell numbers in slices from males did not change significantly with CGRP treatment. Scale bars are 10μm.

A striking modulatory effect of the immune axis was observed when slices were given CGRP containing media. Exposing PCLS to CGRP resulted in a 120% increase in number of $CD19^+$ B cells in slices from females (Figure 2d, f; $P = 0.03$; $n = 9$ 24 h CGRP vs 24 vehicle) but not male mice (Figure 2a, c; $P = 0.97$; $n = 8$ 24 h CGRP vs 9 vehicle) within 24 h of treatment with 10μM CGRP. Within 48 h of 10μM CGRP exposure, the $CD19^+$ B cell population reverted to numbers comparable to vehicle treated controls across five days ex vivo of vehicle treatment in females (Figure 2f; $P = 0.02$; $n = 6$ 48 h CGRP vs 24 Vehicle). Consistent with these observations, $CD19^+$ B cells regularly co-localize with CGRP fibers (Figure 2g). In slices from males, there was

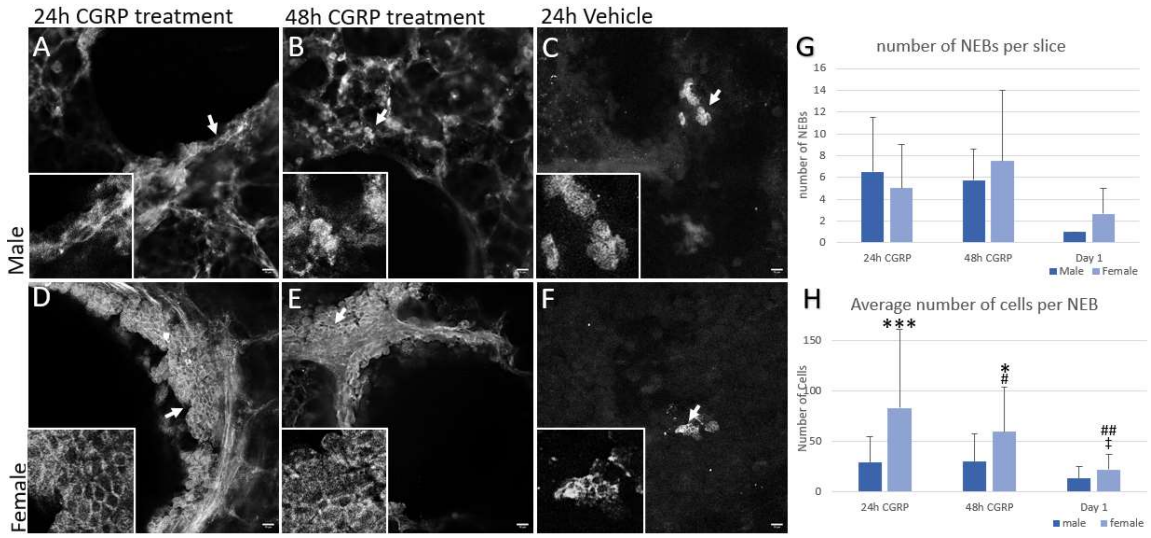

Figure 3: The number of neuroendocrine bodies (NEBs) did not change upon treatment with calcitonin gene related peptide (CGRP) over 24 or 48 h of CGRP treatment and there was no sex difference in number of NEBs. Size of NEBs measured by the number of cells per NEB increases in females at 24 and 48 h of CGRP treatment compared to vehicle. NEBs in slices from females were bigger than males when exposed to CGRP at 24 and 48 h. There were no significant changes in the size of NEBs in slices from males. * Indicates significance between males and females. # Indicates significance compared to 24 h of the same sex, ‡ indicates significance compared to 48 h of the same sex. A-C Male representative images of NEBs. D-F Female representative images of NEBs. Scale bars are 10μm.

no obvious change in $CD19^+$ B cell population compared with vehicle (Figure 2b/c; P = 0.84; n = 8 24 h CGRP vs 9 vehicle). There was no significant difference between male (n = 8) and female (n = 9) slices treated with CGRP at 48 h (Figure 2a-c compared to figure 2d-f; P = 0.94).

NEBs in slices from females were larger after treatment with CGRP. The number of cells per NEB in slices from females was over four times greater after 24 h of CGRP exposure (P = 0.0003; n = 5) (Figure 3d, f) and three times greater after 48 h of CGRP exposure (P = 0.04; figure 2e, f; n = 5) compared to vehicle (n = 20). The number of cells per NEBs in male slices were similar at 24 h (P = 0.33; figure 3a, c; n = 6 24 h CGRP vs 12 vehicle) and 48 h of CGRP treatment to vehicle (P = 0.31; figure 3b, c; n = 6 48 h CGRP vs 12 vehicle). The number of cells per NEB in slices from female lungs

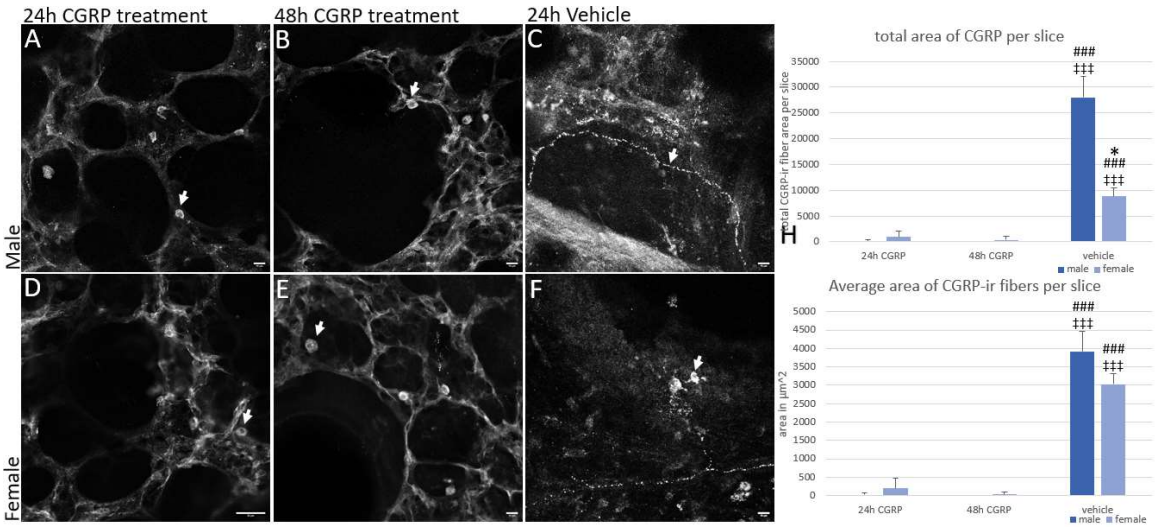

Figure 4: Calcitonin gene related peptide immunoreactive (CGRP-ir) fibers disappeared when treated with CGRP. Pulmonary neuroendocrine cells were still present. # Indicates significance compared to 24 h of the same sex, ‡ indicates significance compared to 48 h of the same sex. A-C. Lung slices from males labeled with CGRP and exposed to CGRP for 24- or 48 h compared to vehicle. D-C. Lung slices from females labeled with CGRP treated with CGRP for 24- or 48 h compared to vehicle. Scale bars are 10µm.

with 24 h of CGRP exposure was almost three times greater than the number of cells per NEB in a 24 h CGRP exposed slice from male lung (P = 0.0004; figure 3a, d; n = 5 female vs 6 male). The number of cells per NEB in 48 h CGRP exposed slices from

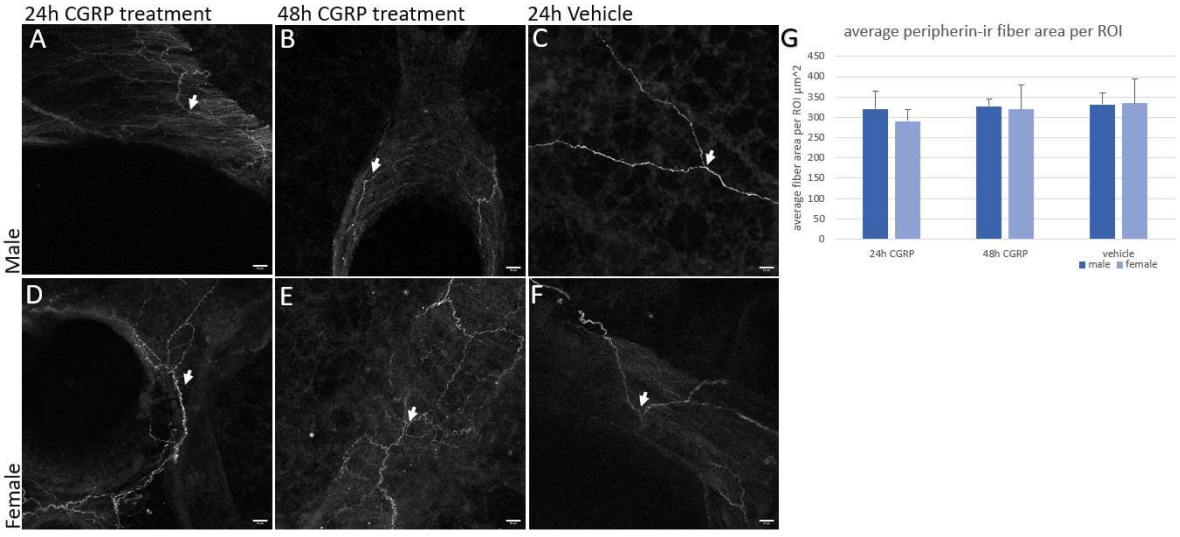

Figure 5: Peripherin fiber area per ROI did not change when exposed to CGRP. A-C. Lung slices from males examined for immunoreactive (ir) peripherin exposed to CGRP for 24- or 48 h compared to vehicle. Lung slices from females examined for ir-peripherin exposed to CGRP for 24- or 48 h compared to vehicle. Scale bars are 25µm.

females was almost two times greater than in similar slices from males (P = 0.03; figure 2b, e; n = 5 female vs 6 male).

Exposing lung slices to exogenous CGRP virtually eliminated ir-CGRP in fibers ex vivo. The average combined area of CGRP-ir fibers per ROI approached zero in

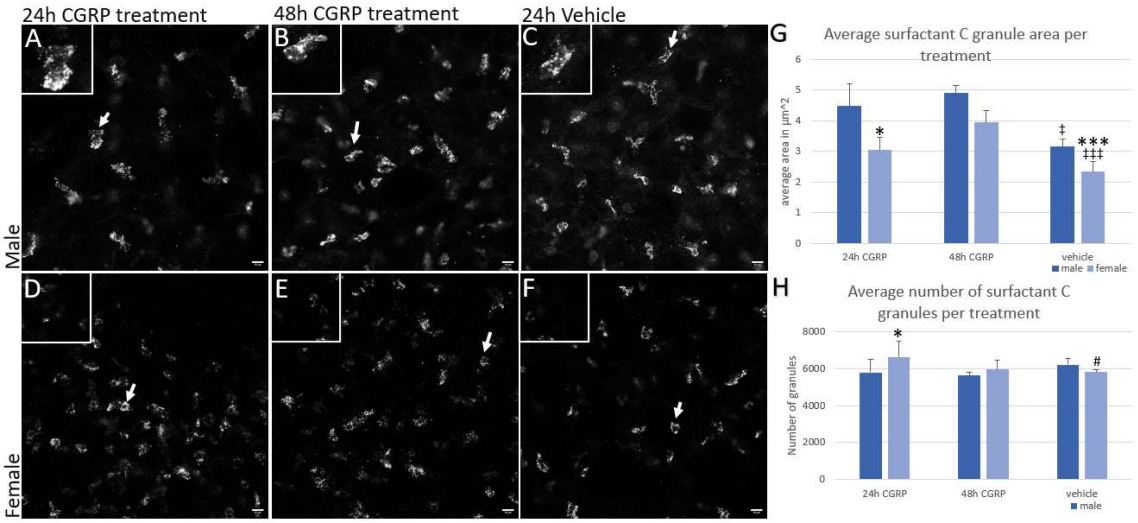

Figure 6: Area of SPC granules significantly increased for slices from females when exposed to CGRP over 48 h. In slices from females immunoreactive (ir) SPC granules were significantly smaller than those in slices from males at 24 h and in vehicle. Number of ir-SPC granules was increased in females at 24 h of CGRP exposure compared to vehicle. * Indicates significance between males and females. # Indicates significance compared to 24 h of the same sex, ‡ indicates significance compared to 48 h of the same sex. A-C. Lung slices from males were examined for ir-SPC exposed to CGRP for 24- or 48 h compared to vehicle. D-F. Lung slices from females were examined for ir-SPC exposed to CGRP for 24- or 48 h compared to vehicle. Scale bars are 10µm.

10µM CGRP exposed tissue over 24 h and 48 h compared to vehicle (Figure 4c, f) for both males (Figure 4a-c; P < 0.0001; n = 5) and females (Figure 4d-f; P < 0.0007; n = 6). However, when treated with 10µM CGRP for 24 h (Figure 5a, d) or 48 h (Figure 5b, e), the average area of peripherin fibers per ROI were similar to vehicle (Figure 5c, f; P = 0.62; n = 13) and was not different between slices from males (Figure 5a-c; n = 7) and females (Figure 5d-f) PCLS (P = 0.79; n = 9).

Type 2 pneumocyte populations indicated by ir-SPC were significantly greater in

area after 48 h of 10μM CGRP exposure compared to vehicle for both male (P = 0.01; n = 7) and female (P = 0.0008; n = 7) PCLS (Figure 6g). The size of granules containing ir-SPC in slices from females were significantly smaller than in males at 24 h of 10μM CGRP treatment (P = 0.017; n = 8 female, 6 male) and in the vehicle (P = 0.0004; n = 21 female, 18 male). The number of granules in slices from females was significantly increased at 24 h of 10μM CGRP exposure compared to vehicle (P = 0.031; n = 8 24 h CGRP, 21 vehicle). The number of granules in slices from females was significantly greater than the number in male slices when treated for 24 h with 10μM CGRP (Figure 6h; P = 0.027; n = 8 female, 6 male). Reference images for SPC labeled male (Figure 6a-c) and female (Figure 6d-f) PCLS are provided for 24 h CGRP (Figure 6a, d) 48 h CGRP (Figure 6b, e), and vehicle (Figure 5c, f) treatments.

Discussion

Exposure of lung tissue to CGRP results in several immunological, physiological, and neural changes in lung tissue. These changes in local neural and immunological signaling pathways are more readily observable using an ex vivo PCLS model that eliminates influences from other organs. The current study demonstrated changes in B cell populations, number of surfactant granules, and NEB size increase in slices from females after 24 h of exposure to 10 μM CGRP. In parallel to these findings, lung slices from females contained a smaller CGRP-ir fiber population than in slices from males and these CGRP-ir fiber populations disappeared after treatment with CGRP in slices from both sexes. Observed sex dependent changes caused by CGRP exposure were consistent with sexually differentiated respiratory disease related responses (Klein and Flanagan 2016; Jacobsen and Klein 2021; Ursin and Klein 2021). The disappearance of

the fibers containing ir-CGRP, in conjunction with the retention of those containing ir-peripherin may indicate an efflux of CGRP and subsequent lack of detectable signal from fibers rather than a loss of fibers themselves. The current study addressed the role of CGRP neuronal signaling with immune and epithelial components using PCLS maintained ex vivo for five days. While in vivo studies have previously reported a diversity of neuropeptide producing fibers in the lung, PCLS studies have rarely reported the diversity of neuropeptides and neurotransmitters observed in the current study (Schleputz et al. 2012). CGRP was detected in neuronal fibers and in PNECs, a unique epithelial endocrine cell population, consistent with previous literature (Mou et al. 2021; Cutz 1982). When exogenous CGRP was added to lung slices, changes in several lung cell characteristics were observed dependent upon the sex of the animal.

A major finding of the current study is that exposure to exogenous CGRP results in an increase in $CD19^+$ B cell populations in slices obtained from females, but not males. These $CD19^+$ B cells were found in germinal centers in PCLS maintained ex vivo across a 5-day period, providing evidence of bronchiolar associated lymphoid tissues (BALT) maintenance, and allowing for exploration of resident immune cell populations in this model. Exogenous CGRP addition resulted in higher numbers of $CD19^+$ B cells throughout female lung slices, not just in BALT. Cell dispersion was likely responsible for an exit of B cells from germinal centers/BALT located primarily in arteriole bronchiole junctions. These B cell movements and behaviors are similar to the propagation of airway epithelial cells in response to injury caused by inhalants or lipopolysaccharide (Oslund et al. 2009; Zhou et al. 2013). Because of the similarities between extracellular CGRP exposure and innate pulmonary response to injury or infection, it may be

possible that CGRP release is a key component of the lung tissue repair processes. This prediction is further substantiated by the known increase of serum CGRP in response to capsaicin and LPS (Durham 2006). The static nature of B cell anatomy and localization over five days without treatments suggests that damage caused to tissue by slicing did not result in any significant immune responses and thereby minimal release of cytokines that would otherwise be released from damaged cells (Henjakovic et al. 2008). Other factors that cause $CD19^{+}$ B cell proliferation in conjunction with cytokine signaling are antigen binding or stimulation from an activated helper T cell (Ollila and Vihinen 2005; Janeway 2001). However, there was no evidence of T cell proliferation in the slices based on CD3 immunoreactive T cells (data not shown).

CGRP exposure increased the number of cells in NEBs, and the quantity of NEBs in tissue increased in slices derived from females but not males. PNECs move to form NEBs, but clustered cells within NEBs can also proliferate, and have been implicated in lung cancers and exhibit stem cell functions (Chen et al. 2019; Gutierrez and Boada 2018; Ouadah et al. 2019). Further, PNECs are known to increase in response to hypoxia and viral disease (Shivaraju et al. 2021; Chen et al. 2019; Benson et al. 2013; Kawanami et al. 2009). The number of PNECs and PNECs per NEB in control tissue were comparable to previously reported values. In CGRP treated tissue the data showed similar numbers of free PNECs compared to control tissue, but an increase in number of PNECs per NEB in females (Ouadah et al. 2019; Branchfield et al. 2016), pointing towards the larger cell counts being indicative of proliferation. PNECs can act as chemo sensors that release neuropeptides and hormones which are known cause various changes to lung physiology tissue remodeling and activation of immune

response (Gu et al. 2014; Cutz 1982; Kaczynska et al. 2018; Song et al. 2012). Stimuli which are correlated with an increase in NEB size such as capsaicin exposure or bacterial infection also increase the amount of serum and tissue CGRP (Russell et al. 2014; Jean et al. 2022; Sui et al. 2018; Bigal, Walter, and Rapoport 2015), consistent with the CGRP induced NEB size increase observed in the current study. Given the colocalization of CGRP fibers with neuroendocrine relevant cells containing neuropeptides and hormones, PNECs and NEBs may act to facilitate the observed neural driven immune response (Noguchi, Furukawa, and Morimoto 2020; Carey, Card, Voltz, Arbes, et al. 2007) that was sex dependent in lung slices.

In conjunction with the changes caused by CGRP to immune and neuroendocrine cell populations, ex vivo CGRP addition resulted in virtual elimination of neuronal fibers containing ir-CGRP. To test whether CGRP exposure resulted in removal of fibers carrying ir-CGRP or whether the exposure simply caused release of ir-CGRP but with fibers still present, a more general marker for peripheral neuronal fibers was examined; ir-peripherin at 24- and 48 h ex vivo. Exposure to CGRP did not reduce the quantity of peripherin-ir fibers. Therefore, it is unlikely that the previously ir-CGRP fibers were eliminated from the slice via degradation. Instead, this disappearance may suggest a positive feedback loop of CGRP release from CGRP-ir fibers upon interaction with the peptide; meaning that CGRP is released when CGRP is externally present (e.g., pre-‘synaptic’ receptors). Conversely, ir-CGRP was not lost from PNECs or NEBs after treatment with exogenous CGRP and no visual increase in PNEC or NEB fluorescent intensity was observed. The retention of ir-CGRP in PNECs versus neuronal fibers may indicate a difference in the presence of a receptor across these cell types.

Ex vivo treatment with CGRP increased SPC-ir granule size and number, suggesting an effect on AT2 cell quantity and function. While CGRP has previously shown to induce epithelial cell proliferation in cell lines, changes in SPC granule number and size have rarely been reported in PCLS (Dakhama, Larsen, and Gelfand 2004; Li, Cohen, et al. 2020; Oslund et al. 2009; Fu et al. 2010; Kawanami et al. 2009). The change in SPC immunoreactivity in the tissue may indicate a change in tissue alveolar cell coverage, because a greater number of observed granules and AT2 cells will result in less space for alveolar type 1 (AT1) projections. Comparatively, the increase in average size of granules indicates a higher level of SPC production and potentially secretion. The pneumocyte populations, consist of AT1 and AT2 cells which are responsible for air exchange and lung structure, respectively. The ratio of these two cell types is dynamic. Both AT1 and AT2 cells have been reported to transdifferentiate into the other under certain conditions, to maintain homeostatic activity in the lung (Jain et al. 2015; Wang et al. 2018; Jansing et al. 2017; Rosenblum et al. 1998). The observed change in surfactant production and AT2 cells may suggest that CGRP exposure plays a role in the re-epithelialization process in ex vivo slices which has been shown in several other PCLS models relating primarily to idiopathic pulmonary fibrosis (Kiener et al. 2021; Ptasinski et al. 2021).

Although innervation of the lung has been explored in the past, it has only been minimally studied in a PCLS model. This study demonstrates the potential of PCLS as a model for investigating peripheral neuro-immune interactions. The nervous innervation of the lung is implicated in various defensive mechanisms against disease utilizing neuropeptide release. Further, there is an implication that neuronal exposure to

neuropeptides results in release of subsequent diverse neuropeptides resulting in complex reactions. For example, one known interaction between substance P, VIP, and CGRP can modulate inflammatory reactions such as mucus secretion in the lung (Atanasova and Reznikov 2018; Chang et al. 2015). VIP, substance P, and CGRP are all located in part around airways and maintain this vicinity in the precision cut lung slices utilized in these experiments. In the current study, neuronal fibers and immunoreactive neuropeptides were maintained ex vivo for over 5 days, making the model more complete than some other PCLS models. The current PCLS protocol allowed for up to sixty parallel slices from the same mouse providing for significant within mouse controls. This made it easier to consider differences caused by environmental stressors, differential microbiota, and other factors that may change from mouse to mouse.

In summary, addition of lung-injury-levels of CGRP to PCLS results in proliferation of $CD19^+$ B cells, increase in size of NEBs, increase in the number of surfactant C granules, and a disappearance of CGRP immunoreactive fibers. These immunological, physiological, and neurological changes occurred in a sex dependent manner. Furthermore, the technical advance of the current slice model allowed the demonstration of neuronal components in the lung that had not been previously demonstrated for CGRP fibers. Using PCLS for neuroimmune lung axis studies allows for exploration of internal lung circuits and will lead to a higher understanding of neuroimmune involved disease response in the future.

Chapter Three/Assessing the Stability and Local Response to Porous Protein Microcrystals in Precision Cut Lung Slices[2]

Graphical Summary:

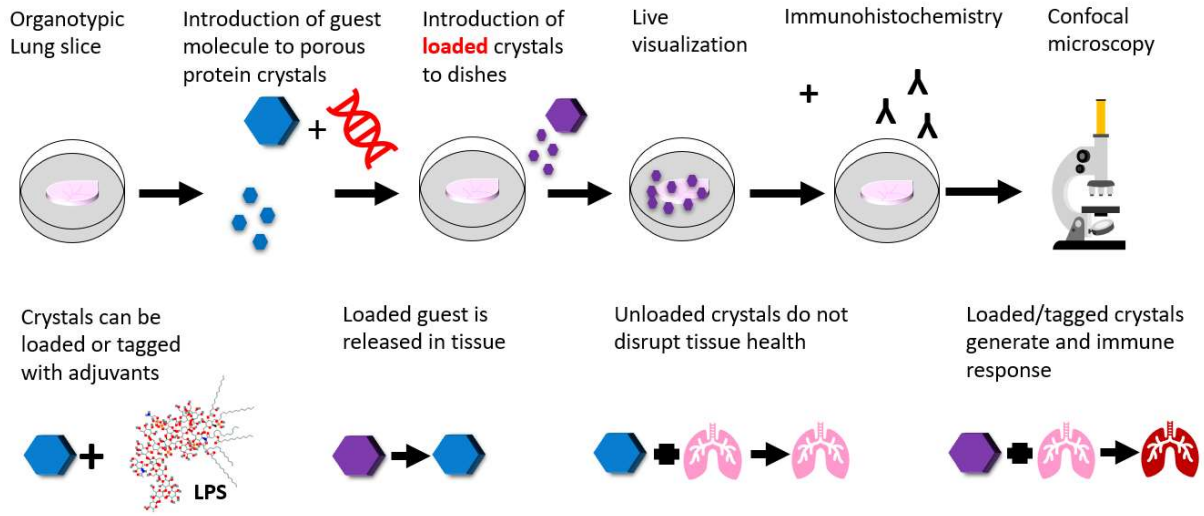

Figure 7: Graphical Summary of Chapter

[2] Authors: Brielle Patlin, Alec A. Jones, Christopher D. Snow, Stuart A. Tobet

Author information:

1. B. Patlin, Department of Biochemistry and Molecular Biology, Colorado State University, Fort Collins, CO.
2. A. Jones, School of Biomedical Engineering and Dept of Biomedical Sciences, Colorado State University, Fort Collins, CO.
3. C. Snow, Department of Chemical and Biological Engineering, Colorado State University, Fort Collins, CO.
4. S. Tobet, School of Biomedical Engineering and Dept of Biomedical Sciences, Colorado State University, Fort Collins, CO.

Overview:

While there are a variety of different drug delivery methods which vary in time of release and location, the method which has produced the greatest interest in the last decade is intranasal drug delivery. This method would immunize the nose and throat membranes as well as lung without the systemic challenges common to oral or injected drugs. This method currently faces a variety of challenges such as difficulty transporting such drugs do to their temperature sensitive natures and the liability of the current delivery mechanism: lipoparticles, to be absorbed by lipid membranes. One way to overcome these challenges is to utilize mesoporous protein crystal scaffolds that contain a loaded guest. Fluorescently labeled crystals can be visualized separately from fluorescently labeled guest in lung tissue. These crystals have been shown to slowly release nucleic acids when introduced to precision cut lung slices. It has further been shown that the crystals are not cytotoxic, and do not trigger an immune response from the tissue. Furthermore, the crystals can be loaded with lipopolysaccharide (LPS), a component of the bacterial cell wall which can trigger an immune response. Administration of fluorescently labeled LPS in crystals, compared to a soluble LPS control, demonstrates release from crystals via generation of B cells. Tissue maintained health demonstrated by a consistent level of permeable (apoptotic or mitotic) cells measured in a slice and crystal structure was not degraded over time. These results demonstrate the potential of porous protein microcrystals as a delivery vehicle for pharmaceutical compounds.

Introduction

We previously demonstrated that a 19.1 kDa trimeric periplasmic polyisoprenoid-binding protein from Campylobacter jejuni (CJ), could be reproducibly produced in E. coli. These “CJ” crystals can be grown to diameters above 100 μm, and smaller than 200 nm, by altering the batch growth conditions – in particular, total protein concentration, precipitant concentration, and pH (Hartje et al. 2017). Crystals composed of proteins can be loaded with a guest and have a variety of potential biological applications. They are uniquely adept at adsorbing nucleic acids with strong binding affinity (Hartje et al. 2018), but can also be loaded with other cargo. An objective of the current study was to test the ability of porous CJ nanocrystals for precision cargo delivery in a biological target tissue.

To determine biological compatibility of CJ crystals the current study chose an ex vivo organotypic slice culture approach as a test bed. Considering a respiratory system end use case, we chose organotypic lung slices (Schwerdtfeger, Ryan, and Tobet 2016; Patlin 2022).This provides the basis for future utilization of live animal models with less risk (Frohlich 2018; Pearson 1986). Chronic obstructive pulmonary disease, by itself, is the third leading cause of death in the world (Mathers, Boerma, and Ma Fat 2009; Lopez and Mathers 2006; Lopez et al. 2006). Improved nasal delivery mechanisms that target the lung are needed to improve therapeutic efficacy (Newman 2017; Labiris and Dolovich 2003a, 2003b; Zhang et al. 2022). CJ crystals generated from protein may provide improved delivery of therapeutic cargoes over other options.

To test cargo compatibility and capacities of the crystals several relevant compounds were chosen, including nucleic acids and proteins. One specialty compound was lipopolysaccharide (LPS): a glycolipid found in the cell wall of gram-negative bacteria (Henjakovic et al. 2008; Kokoszynska et al. 2021). The lipid component is distinctive based on the bacterial origin and provides a potent immunostimulant function. LPS was chosen here because the innate immune system is primed to react against it (Anand and Mande 2018; Kaul et al. 2020; Hussain et al. 2021). By providing LPS as cargo, B cell proliferation provided a direct assessment of stimulated immune signaling (Xu et al. 2008; Venkataraman et al. 1999; Feng et al. 2020). Interestingly, because of its immune stimulatory properties, LPS has previously been used as a vaccine adjuvant (Chilton et al. 2013; Melssen et al. 2019; Casella and Mitchell 2008). In this study, therefore, CJ crystals were evaluated for evidence of decomposition in contact with lung tissue as well as the influence of crystals with different cargoes on lung health. LPS cargo induced immune responses and changes in the number of B cells, cell death, and morphology between LPS, LPS loaded crystal, and control crystal groups were assessed.

Materials and Methods

Animals

Male and Female adult C57BL/6J mice were used. Mice were housed by Laboratory Animal Resources in the Pathology Building at Colorado State University. Mice were multi-housed in plastic cages with aspen bedding (autoclaved Sani-chips; Harlan Teklad, Madison, WI) with a 12:12-hour light-dark cycle and access to water and food (no. 8640; Harlan Teklad).

Precision Cut Lung Slice Preparation

Slices were prepared similarly to previous work (Schwerdtfeger, Ryan, and Tobet 2016).Adult C57BL6/J Thy1-YFP mice were anesthetized using isoflurane and decapitated. Animals were perfused through the heart with warm phosphate buffered saline (PBS). The lungs were inflated using 1ml of 40°C 2% low melting point agarose in MQH2O until the lung was visibly inflated to the edge of the lung without rupturing it. A lung lobe was sliced at 250µm using a vibrating microtome (VT1000S; Leica Microsystems, Wetzlar, Germany). Slices were cultured in phenol red-free lab-made adult neurobasal culture media made with 4mM glucose and L-cysteine reduced to 175µm (Smith et al. 2021) with 2% B27 supplement (Life Technologies; https://www.thermofisher.com/order/catalog/product/17504044;CTS+B27 cell culture media) with a collagen overlay composed of vol/vol: 10.4% 10× MEM, 1.9% PS, 4.2% sodium bicarbonate, and 83.5% collagen (PureCol; Inamed, Fremond, CA). Slices were cultured for up to five days with daily media changes. Slices from three animals were used to generate slices for experiments to account for biological variability.

Immunohistochemical Analysis:

After fixation of slices with 4% paraformaldehyde followed by PBS washes free-floating immunohistochemistry was performed. Lung slices were placed in 1% sodium borohydride for 2-hours followed by 3x10-minute PBS washes. The tissue was then blocked using a 5% normal goat serum (NGS; Lampire Biological, Pipersville, PA), 3% hydrogen peroxide and 0.3% Tx solution in PBS for 2-hours with a change of solution at 1-hour. Primary antisera were applied in a solution containing 5% NGS, 0.3%Tx, and

PBS for 120-hours. Before application of fluorophore-conjugated secondary antisera, slices underwent 4x30-minute washes in a 1% NGS, 0.2% Tx, and PBS solution. Slices were exposed to secondary antisera for 24-hours followed by 4x30-minute washes in a 0.02% Tx PBS solution.

Table 2: Antibodies used for immunohistochemistry

Primary Antibody	Source	Secondary Antibodies	Source	Marker for
CD19 2ug/ml	14-0199-82 eBioscience	Cy3 anti-rat 1:500	112-166-003 Jackson ImmunoResearch	B-cells
SPC 1:500	Ab3786 EMD Millipore	Cy3 anti-rabbit 1:500	111-166-045 Jackson ImmunoResearch	Surfactant Protein C

Tissue Health:

Tissue health was assessed by visual inspection of morphology in each experiment. Slices did not have any necrosis and were field bright; they also did not contain any signs of tissue degradation such as fraying edges or visible loss of epithelial or endothelial cells. In addition, to determine the toxicity of the crystals to the tissue, acridine orange was used to visualize nuclear membrane permeable cells via binding to DNA and cells via binding to RNA in all cells(Byvaltsev et al. 2019). Slices were incubated at 37°C with 2μM acridine orange (A1301; Invitrogen, Thermo Fisher Scientific) followed by 3x10-minute washes with lab-made adult neurobasal + B27 media. Slices were then imaged live using a Nikon Te2000 for acridine orange binding

to DNA using a Texas red filter set (fluorescent emission 656) and for binding to RNA using a fluorescein/GFP filter set (emission 533).

Expression and purification of CJ

Large (>50 μm diameter) CJ crystals were grown via sitting drop vapor diffusion, as described previously (Hartje et al. 2018). Briefly, 2.5 μl, containing approximately 30 μg of purified CJ protein, was mixed with 2.5 μL of sitting drop well buffer, before sealing the well and incubating at 4°C for several days. Each well contained approximately 400 μL of buffer; precipitant concentrations ranged from 3.1 M to 3.6 M ammonium sulfate, 100 mM Bis-Tris, at pH 6.0 or 6.5. After growth, individual large crystals were manually looped from the mother liquor, washed several times in 4.2 M trimethylamine-N-oxide (TMAO), then crosslinked in 40 mg/mL 1-ethyl-3-(3-dimethylaminopropyl) carbodiimide hydrochloride (EDAC), dissolved in 4.2 M TMAO, for 1 to 7 days at room temperature. After crosslinking, the crystals were looped into a quench solution (50 mM sodium borate, pH 9.0) and incubated at room temperature for 30 minutes to 1 hour, before storing long-term in 20 mM HEPES, pH 7.4 at room temperature.

Micro- and nanocrystal batches were synthesized as described previously (Hartje et al. 2017; Hartje et al. 2018); in short, one volume of purified CJ protein, concentrated to between 40 and 50 mg/mL, was combined with 5 volumes of precipitant buffer (3.2 M – 3.5 M ammonium sulfate, 100 mM HEPES or Bis-Tris, pH 7.0). The total volume of crystals grown using this method ranged from 240 μL (i.e., 40 μL of protein combined with 200 μL of precipitant buffer) to 720 μL. Crosslinking of micro- and nanocrystals was achieved by first pelleting the crystals via centrifugation (5:00 minutes at 2,000 x g) and

replacing the mother liquor/supernatant with 4.2 M TMAO. After centrifuging again, the supernatant was replaced with 0.5 - 0.75 mL crosslinking buffer (40 mg/mL EDAC, dissolved in 4.2 M TMAO), supplemented with NHS-Pacific Blue dye (Thermo Fisher, P10163) or NHS-Texas Red dye (Thermo Fisher, T20175) at a final concentration of 5 µg/mL. The crystals were allowed to soak in crosslinking buffer for >18 hours at room temperature, with constant rotation. The crosslinking was quenched by replacing the supernatant with EDAC quench buffer (50 mM sodium borate, pH 9) and incubating at room temperature with constant inversions for >30 minutes. The crystals were then pelleted a final time, and the supernatant was replaced with 1X PBS, pH 7.5, and stored at room temperature long-term. All crystals underwent UV irradiation to insure sterility prior to ex vivo live tissue exposure.

Guest Incorporation

For loading of guest nucleic acids, crystals were soaked for greater than 1 hour at room temperature in 1 µM, fluorescein-labeled ssDNA (5'-TAGGCGACTCGACGGTCTTACGCGTTACGT -3'), and subsequently washed in nuclease-free water. Guest fluorescence within the crystals was validated on an Eclipse Ti-E series inverted spinning disk confocal microscope (Nikon), prior to crystal addition to tissue slices. For LPS testing, crystals were incubated at room temperature with 0.1 mg/mL Alexa Fluor 568-LPS conjugate for > 1 hour. After soaking, the crystals were washed once and resuspended in nuclease-free water.

Results

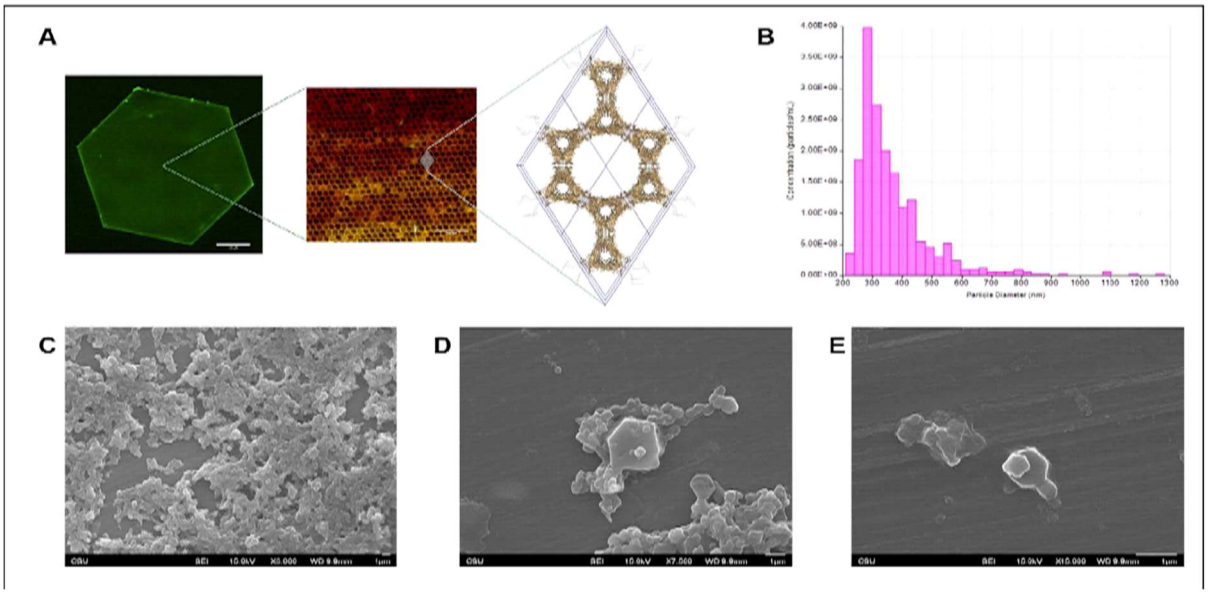

Figure 8: A) Nanocrystals are composed of a hexagonal beehive structure composed of 13nm pores. B) Histogram of crystal size. C)-E) electron micrograph of crystals.

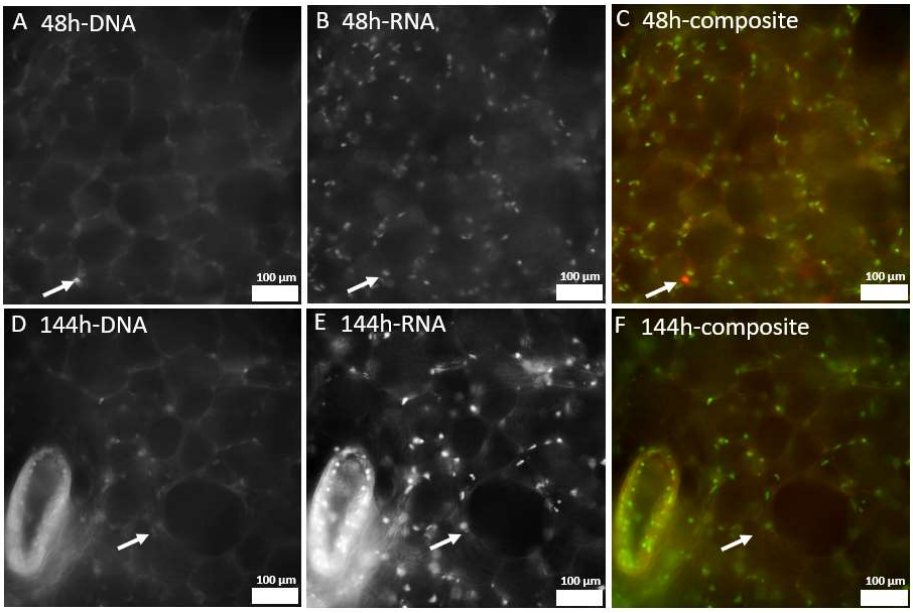

Figure 9. Tissue remains healthy over 4 days ex vivo as demonstrated by consistently low cell death visualized via acridine orange. A) DNA shown in cells with permeable nuclei in the red channel at 48 h ex vivo representing dead cells. B) RNA shown in cells in the green channel at 48 h ex vivo. C) Composite image of A and B. D) DNA shown in cells with permeable nuclei in the red channel at 96 h ex vivo representing dead cells. E) RNA shown in cells in the green channel at 96 h ex vivo. F) Composite image of D and E. G) Visualization of NHS-Pacific Blue labeled crystals.

Porous micro- and nanocrystals are hexagonal structures composed of trimeric subunits. The pores in the crystal are ~13nm in diameter and span the depth of the crystal (Figure 8a). They range in size from 200-1300nm with the majority of crystals approximately 100nm in size (Figure 8b).

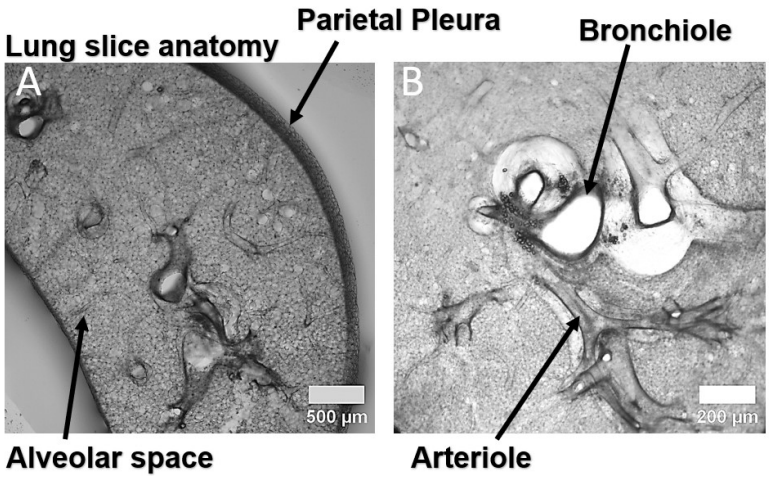

Figure 10. Anatomy of a PCLS. A) Alveolar space and parietal pleura with 500µm scale bar. B. Arteriole and bronchiole with 200µm scale bar.

Lung slices were maintained ex vivo up to a week. Health status of lung slices were observed using a variety of characteristics. Macroscopically, lung slices consisted of the alveolar spaces (where breathing would occur in vivo), the parietal pleura which is the outside wall of the lung (Figure 10a), the airways or bronchioles, and the blood vessels or arterioles (Figure 8b). In all cases, the cells maintained their characteristic shapes and size with no evidence of tissue degeneration. To further demonstrate the health of the tissue unloaded NHS-pacific blue conjugated crystals were utilized to prevent fluorescent overlap with acridine orange (Figure 9g). When treated live with acridine orange, cellular DNA was visualized in the red channel (Figure 9a, d) and RNA was visualized in the green channel (Figure 9b, e). Because acridine orange can cross cellular but not nuclear membranes, in the red channel, this labeling allows visualization

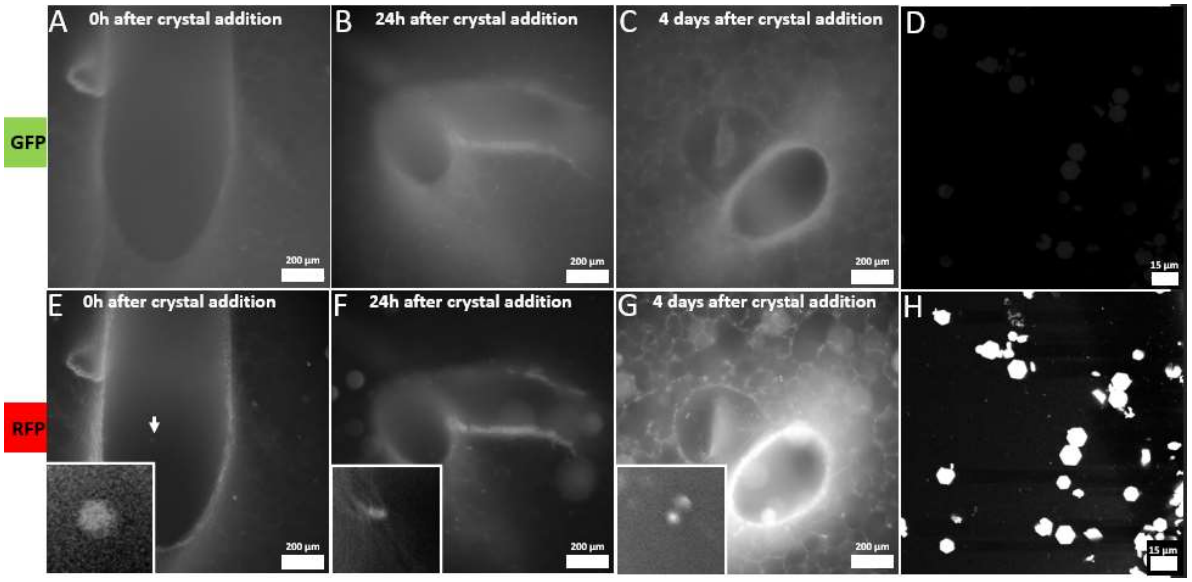

Figure 11. Lung slices exposed to unloaded Texas red labeled micro/nanocrystals. A-C) PCLS imaged live immediately, 24 h, and 96 h after crystal addition show no fluorescence in the green channel and are a control for crystal visualization. Scale bar is 200µm. E-G) PCLS imaged live immediately, 24 h, and 96 h after crystal addition are fluorescent in the red channel and demonstrate a greater number of crystals present in the plane of the tissue over time. Scale bar is 200µm. D) After fixation confocal images of crystals were acquired showing no fluorescence in the green channel and high fluorescence in the red channel. No degradation of crystal fluorescence or structure was observed compared to pre-experiment

of porous nuclear membranes of dead cells. No change in the number of dead cells in a lung slice were observed with crystal addition. Red and green overlays were then generated to show localization of the labeled DNA and RNA populations (Figure 9c, f).

To determine whether the crystals could enter the tissue slices, Texas red labeled crystals were applied on top of the collagen overlay and the progression of crystals into the plane of the tissue was observed by sequential imaging. Live images were taken immediately, 24 h, and 48 h after addition in with a Fluorescein/GFP filter set to visualize all cells containing RNA (Figure 11a-d) and a Texas red filter set to visualize cells with permeable nuclear membranes (Figure 11e-h). This functions as a marker of tissue health by separating out cells which are dead and mitotic from the total population. Crystals were visible in the Texas red channel, but not the fluorescein/GFP

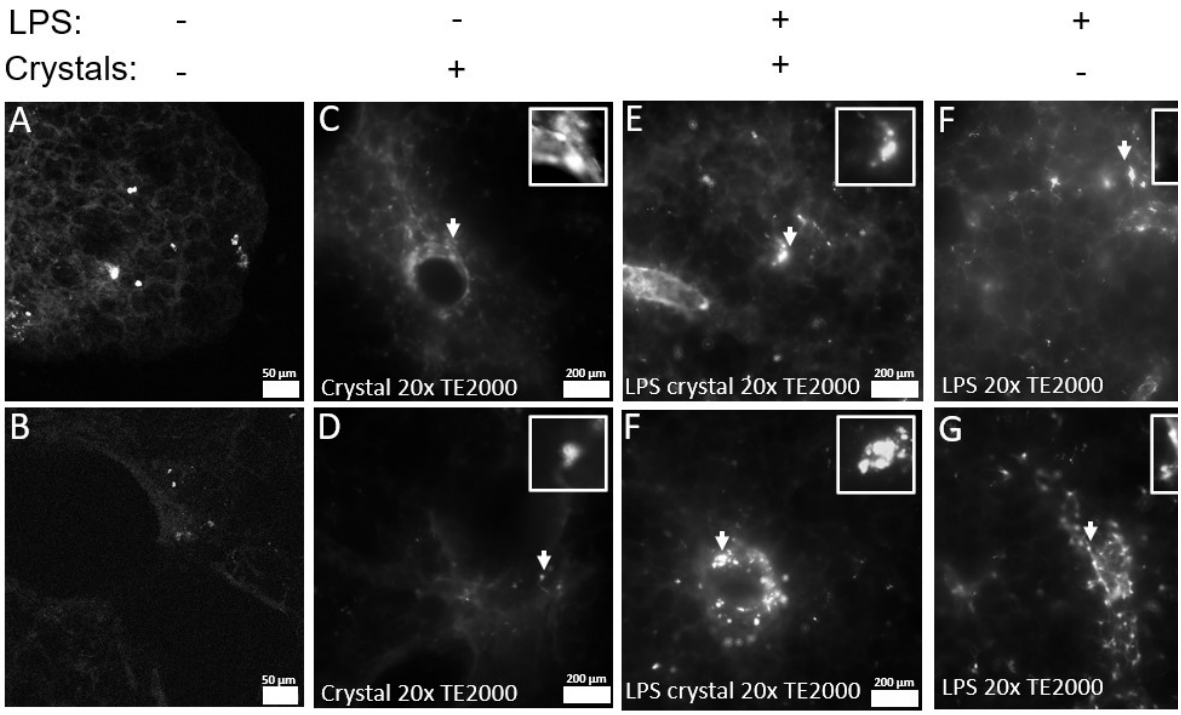

Figure 12. Loading LPS into crystal pores changes the B cell immunomodulatory effects of crystals. A) B cell population 24h ex vivo in PCLS not exposed to crystals (-/-). B) B cell population 48h ex vivo in PCLS not exposed to crystals (-/-). C) B cell population 24h ex vivo in PCLS exposed to unloaded crystals (-/+). D) B cell population 48h ex vivo in PCLS exposed to unloaded crystals (-/+). E) B cell population 24h ex vivo in PCLS exposed to LPS loaded crystals (+/+). F) B cell population 48h ex vivo in PCLS exposed to LPS loaded crystals (+/+). G) B cell population 24h ex vivo in PCLS exposed to LPS in bath (+/-). H) B cell population 48h ex vivo in PCLS exposed to LPS in bath (+/-).

channel). Some crystals fell into the plane of the tissue immediately after addition (Figure 11e) and remaining crystals, arrived over the next several days (Figure 11f-g). After aldehyde fixation, high magnification images of the crystals in the tissue showed no degradation of Texas red fluorescence or crystal structure (Figure 11d, h).

Crystals were loaded with a fluorescein conjugated DNA to demonstrate loading with a biologically relevant molecule. Unloaded crystals were visualized in red and green channels as a z projection 3D image for unloaded (Figure 11a) and loaded crystals (Figure 11b). Texas red labeled crystals loaded with a fluorescein conjugated DNA were yellow in lung tissue.

Crystals did not cause an immune modulatory effect in lung tissue (Figure 12c-d) compared to tissue without crystals (Figure 12a-b). LPS applied via bath (Figure 6g-h) results in a much higher B cell population increase than crystals loaded with LPS (Figure 12e-f). Slices generated from female mice had a higher B cell population growth than slices generated from male mice.

Discussion

In the current study, PCLS were used to test the biocompatibility of CJ crystals with live organ tissue. When LPS was loaded into crystals as cargo, there was an apparent proliferation of B cells in the slices. This B cell population increase was less than the population increase generated by treating PCLS with LPS in the media that likely indicates a restricted release mechanism from the crystals. Conversely, unloaded crystals added to PCLS did not influence normal B cell populations. These comparable populations indicate that the crystals themselves did not have an immunomodulatory effect across 48 h. One benefit of the crystals being inert when testing them for use in the lungs is that they will not contribute to the overactivated immune system pathology common to many respiratory diseases. The crystals can be loaded with a broad range of biologically relevant substance such as nucleic acids and proteins which makes them a potential drug delivery mechanism for a broad range of pharmaceuticals. Pore sizes, which can be regulated in the synthetic steps, can be large meaning that the size of cargo can be relatively large compared to other models.

As seen previously (Patlin 2022), healthy tissue was noted after several days without added crystals and the addition of crystals by themselves did not change any aspect of

tissue health. Crystals clearly penetrated the porous protective polymer that covers the PCLS over 96 hours with some immediate deposition that increased over time. Total delivery of crystals was not accomplished, but this effect mirrors the effect of applying a drug nasally, because the mucociliary ladder will prevent complete delivery making it a better model for nasal drug delivery. There were no increases in cell death in unloaded crystal treated slices visualized across 96 h, and no change in B cell population observed in unloaded crystal treated PCLS compared to vehicle treated. The effects of LPS-loaded crystals on B cell populations that are representative of immune responses in PCLS indicates the utility of CJ crystals as a potential drug delivery vector.

The current study was conducted to determine whether there were any adverse effects of CJ crystal in live tissue (ex vivo) (Zhang et al. 2022; Schuster, Laggner, and Langer 2005; Zhang et al. 2013). There was potential for CJ crystals to negatively interact with tissue due to the proteins' microbial origin. As a polyisoprenoid binding protein it was possible that it could bind to something in mammalian tissue. Further, the synthetic process of crystal formation may have rendered the material toxic to live tissue (e.g., bacterial contamination). In all situations studied, the crystals were inert there were no inappropriate infections; only LPS as cargo induced a physiological response.

Based on the results of the current study, CJ crystals may provide a useful vaccine delivery vector. Such a vector should be able to deliver an antigen to the host immune system. A vaccine delivery vector should be able to maintain the stability of the vaccine during storage and transport. This can help to ensure that the vaccine remains effective and retains its potency until it is ready to be administered; this is especially relevant in settings where maintaining cold-chain supply is not feasible. Crystals are stable above

freezing temperatures and may be able to prevent guest molecules from degrading in transport.

In the current study, PCLS was used to study the efficacy of porous nanocrystals as drug delivery devices. Crystals interacted with the PCLS without affecting health as visualized by maintenance of gross morphological characteristics of the tissue, the B cell immune population, or cell death. Crystals were loaded with LPS, an immune stimulator that can be used as a vaccine adjuvant. The LPS loaded crystals resulted significant B cell activation. The activation was less compared to LPS added directly to the media suggesting that the crystals provided for restricted release. In conclusion, porous protein micro/nanocrystals have potential as a drug delivery mechanism going forward.

Chapter Four/Conclusions

PCLS are an increasingly useful model for studying topics relevant to respiratory disease. They contain diverse cell type populations and maintain the 3D scaffold structure and extracellular matrix of an actual lung. Cell-cell and cell-extracellular interactions are maintained and therefore PCLS are extremely biologically relevant. They have also recently been shown to be a useful model for drug development, bridging the gap between in vitro and in vivo models. This model is imperative for studying respiratory diseases that affect all systems in the lung. Many aspects of respiratory disease have yet to be explored. For example, interactions between the nervous system and the immune populations in the lung are rarely explored ex vivo, and although the model is useful for drug development, it is just beginning to be used for that purpose.

In the studies presented here, experiments exploring these understudied aspects of disease were explored in PCLS in a sex selective manner with a focus on immune change indicated primarily by B cell population changes. In the first study, the signaling effects of the peptide CGRP were examined in relation to the physiological, immunological, and neural populations of the lungs. In the second study, the use of PCLS as a platform for studying drug delivery and the potential of porous protein crystals was assessed for a role in drug delivery.

Although innervation of the lung has been explored in the past, it has only been minimally studied in a PCLS model. Chapter 2 demonstrates the potential of PCLS as a

model for investigating peripheral neuro-immune interactions. The nervous innervation of the lung is implicated in various defensive mechanisms against disease utilizing neuropeptide release. There is an implication that neuronal exposure to neuropeptides results in release of subsequent diverse neuropeptides resulting in complex reactions. For example, one known interaction between substance P, VIP, and CGRP can modulate inflammatory reactions such as mucus secretion in the lung (Atanasova and Reznikov 2018; Chang et al. 2015). VIP, substance P, and CGRP are all located in part around airways and maintain this vicinity in the precision cut lung slices utilized in these experiments. In the current study, neuronal fibers and immunoreactive neuropeptides were maintained ex vivo for over 5 days, making the model more complete than some other PCLS models. The current PCLS protocol allowed for up to sixty parallel slices from the same mouse providing for significant within mouse controls. This made it easier to consider differences caused by environmental stressors, differential microbiota, and other factors that may change from mouse to mouse.

Addition of lung-injury-levels of CGRP to PCLS resulted in proliferation of $CD19^{+}$ B cells, increase in size of NEBs, increase in the number of surfactant C granules, and a disappearance of CGRP immunoreactive fibers. These immunological, physiological, and neurological changes occurred in a sex selective manner. The technical advance of the current slice model allowed the demonstration of neuronal components in the lung that had not been previously demonstrated for CGRP fibers. Using PCLS for neuroimmune lung axis studies allows for exploration of internal lung circuits and will lead to a higher understanding of neuroimmune involved disease response in the future.

In chapter three I showed that PCLS can be used to study the efficacy of porous microcrystals as a drug delivery device. Crystals interact with the PCLS and do not affect health as visualized by no change in morphology, the B cell immune population, or cell death. Crystals then can be loaded with an adjuvant molecule known as LPS. The LPS loaded crystals then result in a lower level of B cell activation compared to LPS in the media of the PCLS.

Change in B cell population size can be induced in the lungs by delivery of LPS via micro/nanocrystals. This B cell population increase was less than the population increase generated by treating PCLS with LPS in the media which may indicate a partial or slow-release mechanism from the crystals. Conversely, PCLS treated with unloaded crystals have normal B cell populations compared to vehicle treated PCLS. These comparable populations indicate that the crystals themselves do not have an immunomodulatory effect across 48 h. One benefit of the crystals being inert when testing them for use in the lungs is that they will not contribute to the overactivated immune system pathology common to many respiratory diseases. However, the crystals can be loaded with a broad range of biologically relevant substance such as nucleic acids and proteins which makes them a potential drug delivery mechanism for a broad range of pharmaceuticals. Further, the size of the pore is large meaning that the size of loadable contents can be relatively high compared to some other models. Porous protein micro/nanocrystals therefore have great potential as a drug delivery mechanism in the future.

Although some changes related to CGRP exposure were elucidated, more functions and molecular mechanisms have yet to be explored. Sex differences also

need to be further studied due to the significant history of differences in respiratory disease and the dearth of sex selective neuronal signaling leading to immune response in the lungs. These experiments could include hormonal influences on CGRP signaling, sex differences in other immune populations, or characterization of changing transcripts produced in the lungs of male and female mice relevant to CGRP. Other neuropeptide effects could also be assessed both separately and in tandem. Another line of study which needs to be explored is the role of bacteria in the lung on the lung-gut axis. There are several connections between the gut and the lungs both in terms of blood flow and neural fibers. Because it has become clear that the lungs are not a sterile organ, and contain a thriving microbiome, the effects of different bacterial populations need to be assessed in reference to neurological signaling in the lung. The neuroimmune axis of the gut plays a vital role in respiratory disease response.

In terms of studying drug delivery mechanisms, it will be important in the future to determine the protective nature of the crystals, because of the current difficulties with maintaining proper temperatures and conditions for drug efficacy. Other cellular populations should also be explored and the polyisoprenoid protein which composes the crystals may have some unintended affects which should be verified. Because it is relatively immunologically inert, the crystals should be tested for ability to uptake a broader range of biologically relevant molecules with properties such as hydrophobicity/hydrophilicity, size, and stability.

Respiratory disease, treatment, and innate immune response in the lung are highly complex. Therefore, it is useful to have a model which can simplify some of the variables by eliminating extra signaling from outside the lung while maintaining the in-

organ interactions. By adding sensors, the model can be adapted to assess lung metabolism to increase the range of information that can be collected. Our PCLS model has broad ranging potential uses in drug development and in understanding respiratory diseases. These slices also have great potential for studying infectious disease. It is more humane to study these diseases ex vivo, but cell lines do not provide enough translational relevance. Facets of this model such as the maintenance of the 3-dimensional structure and intercellular interactions make it ideal for studies of dangerous respiratory pathogens. It is also relevant for determining adverse side effects in other parts of the lung and exploring the role of over- and under-active immune responses related to respiratory disease progression. PCLS can also be generated from explants that may make them a possible diagnostic tool in the future. They could be instrumental for studying future pandemic level threats. Large scale infectious events tend to be respiratory in nature and this model will speed up understanding the disease and developing treatments for the future.

References

Alsafadi, H. N., F. E. Uhl, R. H. Pineda, K. E. Bailey, M. Rojas, D. E. Wagner, and M. Konigshoff. 2020. 'Applications and Approaches for Three-Dimensional Precision-Cut Lung Slices. Disease Modeling and Drug Discovery', *Am J Respir Cell Mol Biol*, 62: 681-91.

Anand, S., and S. S. Mande. 2018. 'Diet, Microbiota and Gut-Lung Connection', *Frontiers in Microbiology*, 9.

Assas, B. M., J. I. Pennock, and J. A. Miyan. 2014. 'Calcitonin gene-related peptide is a key neurotransmitter in the neuro-immune axis', *Frontiers in Neuroscience*, 8.

Assas, M. B. 2021. 'Anti-migraine agents from an immunological point of view', *J Transl Med*, 19: 23.

Atanasova, K. R., and L. R. Reznikov. 2018. 'Neuropeptides in asthma, chronic obstructive pulmonary disease and cystic fibrosis', *Respir Res*, 19: 149.

Bai, Y., A. G. P. Guedes, R. Krishnan, and X. Ai. 2022. 'CD38 plays an age-related role in cholinergic deregulation of airway smooth muscle contractility', *J Allergy Clin Immunol*, 149: 1643-54 e8.

Bailey, K. E., C. Pino, M. L. Lennon, A. Lyons, J. G. Jacot, S. R. Lammers, M. Konigshoff, and C. M. Magin. 2020. 'Embedding of Precision-Cut Lung Slices in Engineered Hydrogel Biomaterials Supports Extended Ex Vivo Culture', *Am J Respir Cell Mol Biol*, 62: 14-22.

Barnes, P. J. 2016. 'Sex Differences in Chronic Obstructive Pulmonary Disease Mechanisms', *American Journal of Respiratory and Critical Care Medicine*, 193: 813-14.

Benam, K. H., M. Konigshoff, and O. Eickelberg. 2018. 'Breaking the In Vitro Barrier in Respiratory Medicine. Engineered Microphysiological Systems for Chronic Obstructive Pulmonary Disease and Beyond', *Am J Respir Crit Care Med*, 197: 869-75.

Benemei, S., P. Nicoletti, J. G. Capone, and P. Geppetti. 2009. 'CGRP receptors in the control of pain and inflammation', *Current Opinion in Pharmacology*, 9: 9-14.

Benson, R. E., M. L. Rosado-de-Christenson, S. Martinez-Jimenez, J. R. Kunin, and P. P. Pettavel. 2013. 'Spectrum of pulmonary neuroendocrine proliferations and neoplasms', *Radiographics*, 33: 1631-49.

Bigal, M. E., S. Walter, and A. M. Rapoport. 2015. 'Therapeutic antibodies against CGRP or its receptor', *Br J Clin Pharmacol*, 79: 886-95.

Bindal, R. D., K. E. Carlson, B. S. Katzenellenbogen, and J. A. Katzenellenbogen. 1988. 'Lipophilic impurities, not phenolsulfonphthalein, account for the estrogenic activity in commercial preparations of phenol red', *J Steroid Biochem*, 31: 287-93.

Birkhoff, M., M. Leitz, and D. Marx. 2009. 'Advantages of Intranasal Vaccination and Considerations on Device Selection', *Indian Journal of Pharmaceutical Sciences*, 71: 729-31.

Blake, K. J., X. R. Jiang, and I. M. Chiu. 2019. 'Neuronal Regulation of Immunity in the Skin and Lungs', *Trends Neurosci*, 42: 537-51.

Branchfield, K., L. Nantie, J. M. Verheyden, P. Sui, M. D. Wienhold, and X. Sun. 2016. 'Pulmonary neuroendocrine cells function as airway sensors to control lung immune response', *Science*, 351: 707-10.

Brill, S. E., M. Law, E. El-Emir, J. P. Allinson, P. James, V. Maddox, G. C. Donaldson, T. D. McHugh, W. O. Cookson, M. F. Moffatt, I. Nazareth, J. R. Hurst, P. M. Calverley, M. J. Sweeting, and J. A. Wedzicha. 2015. 'Effects of different antibiotic classes on airway bacteria in stable COPD using culture and molecular techniques: a randomised controlled trial', *Thorax*, 70: 930-8.

Burgstaller, G., M. Gerckens, O. Eickelberg, and M. Konigshoff. 2021. 'Decellularized Human Lung Scaffolds as Complex Three-Dimensional Tissue Culture Models to Study Functional Behavior of Fibroblasts', *Methods Mol Biol*, 2299: 447-56.

Byvaltsev, V. A., L. A. Bardonova, N. R. Onaka, R. A. Polkin, S. V. Ochkal, V. V. Shepelev, M. A. Aliyev, and A. A. Potapov. 2019. 'Acridine Orange: A Review of Novel Applications for Surgical Cancer Imaging and Therapy', *Front Oncol*, 9: 925.

Cadieux, A., N. P. Monast, F. Pomerleau, A. Fournier, and C. Lanoue. 1999. 'Bronchoprotector properties of calcitonin gene-related peptide in guinea pig and human airways. Effect of pulmonary inflammation', *Am J Respir Crit Care Med*, 159: 235-43.

Carey, M. A., J. W. Card, J. W. Voltz, S. J. Arbes, Jr., D. R. Germolec, K. S. Korach, and D. C. Zeldin. 2007. 'It's all about sex: gender, lung development and lung disease', *Trends Endocrinol Metab*, 18: 308-13.

Carey, M. A., J. W. Card, J. W. Voltz, D. R. Germolec, K. S. Korach, and D. C. Zeldin. 2007. 'The impact of sex and sex hormones on lung physiology and disease: lessons from animal studies', *American Journal of Physiology-Lung Cellular and Molecular Physiology*, 293: L272-L78.

Casella, C. R., and T. C. Mitchell. 2008. 'Putting endotoxin to work for us: monophosphoryl lipid A as a safe and effective vaccine adjuvant', *Cellular and Molecular Life Sciences*, 65: 3231-40.

Chamekh, M., M. Deny, M. Romano, N. Lefevre, F. Corazza, J. Duchateau, and G. Casimir. 2017. 'Differential Susceptibility to Infectious Respiratory Diseases between Males and Females Linked to Sex-Specific Innate Immune Inflammatory Response', *Frontiers in Immunology*, 8: 1806.

Chang, R. B., D. E. Strochlic, E. K. Williams, B. D. Umans, and S. D. Liberles. 2015. 'Vagal Sensory Neuron Subtypes that Differentially Control Breathing', *Cell*, 161: 622-33.

Chen, H. J., A. Poran, A. M. Unni, S. X. Huang, O. Elemento, H. W. Snoeck, and H. Varmus. 2019. 'Generation of pulmonary neuroendocrine cells and SCLC-like tumors from human embryonic stem cells', *J Exp Med*, 216: 674-87.

Chilton, P. M., D. M. Hadel, T. T. To, T. C. Mitchell, and R. P. Darveau. 2013. 'Adjuvant activity of naturally occurring monophosphoryl lipopolysaccharide preparations from mucosa-associated bacteria', *Infect Immun*, 81: 3317-25.

Crowe, T. P., and W. H. Hsu. 2022. 'Evaluation of Recent Intranasal Drug Delivery Systems to the Central Nervous System', *Pharmaceutics*, 14.

Cutz, E. 1982. 'Neuroendocrine cells of the lung. An overview of morphologic characteristics and development', *Experimental Lung Research*, 3: 185-208.

Dakhama, A., G. L. Larsen, and E. W. Gelfand. 2004. 'Calcitonin gene-related peptide: role in airway homeostasis', *Curr Opin Pharmacol*, 4: 215-20.

Dallmayer, M., J. Li, S. Ohmura, R. Alba Rubio, M. C. Baldauf, T. L. B. Holting, J. Musa, M. M. L. Knott, S. Stein, F. Cidre-Aranaz, F. S. Wehweck, L. Romero-Perez, J. S. Gerke, M. F. Orth, A. Marchetto, T. Kirchner, H. Bach, G. Sannino, and T. G. P. Grunewald. 2019. 'Targeting the CALCB/RAMP1 axis inhibits growth of Ewing sarcoma', *Cell Death Dis*, 10: 116.

Deen, M., E. Correnti, K. Kamm, T. Kelderman, L. Papetti, E. Rubio-Beltran, S. Vigneri, L. Edvinsson, A. Maassen Van Den Brink, and Studies European Headache Federation School of Advanced. 2017. 'Blocking CGRP in migraine patients - a review of pros and cons', *J Headache Pain*, 18: 96.

Dominelli, P. B., and Y. Molgat-Seon. 2022. 'Sex, gender and the pulmonary physiology of exercise', *European Respiratory Review*, 31.

Dragunas, G., M. E. Woest, S. Nijboer, S. T. Bos, J. van Asselt, A. P. de Groot, E. Vohlidalova, C. J. Vermeulen, B. Ditz, J. M. Vonk, G. H. Koppelman, M. van den Berge, N. H. T. Ten Hacken, W. Timens, C. D. Munhoz, Y. S. Prakash, R. Gosens, and L. E. M. Kistemaker. 2020. 'Cholinergic neuroplasticity in asthma driven by TrkB signaling', *Faseb Journal*, 34: 7703-17.

Durham, P. L. 2006. 'Calcitonin gene-related peptide (CGRP) and migraine', *Headache*, 46 Suppl 1: S3-8.

Durham, P. L., and C. V. Vause. 2010. 'Calcitonin gene-related peptide (CGRP) receptor antagonists in the treatment of migraine', *CNS Drugs*, 24: 539-48.

Enlo-Scott, Z., E. Backstrom, I. Mudway, and B. Forbes. 2021. 'Drug metabolism in the lungs: opportunities for optimising inhaled medicines', *Expert Opinion on Drug Metabolism & Toxicology*, 17: 611-25.

Fang, Z., X. H. Hu, K. Li, J. Han, L. Tian, J. Yan, W. Zhang, W. Q. Lai, B. C. Lin, X. H. Liu, and Z. G. Xi. 2020. '[Inflammatory mechanism of hippocampal tissue injury induced by PM(2.5) in nasal drip in mice]', *Zhongguo Ying Yong Sheng Li Xue Za Zhi*, 36: 240-44.

Feng, B., J. Zhu, Y. Xu, W. Chen, X. Sheng, X. Feng, X. Shi, J. Liu, Q. Pan, J. Yang, J. Yu, L. Li, and H. Cao. 2020. 'Immunosuppressive effects of mesenchymal stem cells on lung B cell gene expression in LPS-induced acute lung injury', *Stem Cell Res Ther*, 11: 418.

Feng, G., R. H. Mellor, M. Bernstein, C. Keller-Peck, Q. T. Nguyen, M. Wallace, J. M. Nerbonne, J. W. Lichtman, and J. R. Sanes. 2000. 'Imaging neuronal subsets in transgenic mice expressing multiple spectral variants of GFP', *Neuron*, 28: 41-51.

Foroutan, F., G. Guyatt, E. Friesen, L. E. C. Lozano, A. Sidhu, and M. Meade. 2019. 'Predictors of 1-year mortality in adult lung transplant recipients: a systematic review and meta-analysis', *Syst Rev*, 8: 131.

Freeman, B. A., and J. J. O'Neil. 1984. 'Tissue slices in the study of lung metabolism and toxicology', *Environ Health Perspect*, 56: 51-60.

Frohlich, E. 2018. 'Comparison of conventional and advanced in vitro models in the toxicity testing of nanoparticles', *Artif Cells Nanomed Biotechnol*, 46: 1091-107.

Fu, H. M., L. Li, Y. J. Wang, C. H. Tang, H. Y. Mi, F. Xu, and F. W. Kuang. 2010. '[The proliferation-promoting effects of calcitonin gene-related peptide on type II alveolar epithelial cell exposed to hyperoxia mediated by protein kinase C alpha pathway]', *Zhongguo Wei Zhong Bing Ji Jiu Yi Xue*, 22: 263-6.

Fuseini, H., and D. C. Newcomb. 2017. 'Mechanisms Driving Gender Differences in Asthma', *Curr Allergy Asthma Rep*, 17: 19.

Gerpe, M. C. R., J. P. van Vloten, L. A. Santry, J. de Jong, R. C. Mould, A. Pelin, J. C. Bell, B. W. Bridle, and S. K. Wootton. 2018. 'Use of Precision-Cut Lung Slices as an Ex Vivo Tool for Evaluating Viruses and Viral Vectors for Gene and Oncolytic Therapy', *Molecular Therapy-Methods & Clinical Development*, 10: 245-56.

Grassin-Delyle, S., A. Buenestado, E. Naline, C. Faisy, S. Blouquit-Laye, L. J. Couderc, M. Le Guen, M. Fischler, and P. Devillier. 2012. 'Intranasal drug delivery: an efficient and non-invasive route for systemic administration: focus on opioids', *Pharmacol Ther*, 134: 366-79.

Gstraunthaler, G., T. Lindl, and J. van der Valk. 2013. 'A plea to reduce or replace fetal bovine serum in cell culture media', *Cytotechnology*, 65: 791-3.

Gu, X., P. H. Karp, S. L. Brody, R. A. Pierce, M. J. Welsh, M. J. Holtzman, and Y. Ben-Shahar. 2014. 'Chemosensory functions for pulmonary neuroendocrine cells', *Am J Respir Cell Mol Biol*, 50: 637-46.

Gurdal, M., O. Barut Selver, K. Baysal, and I. Durak. 2018. 'Comparison of culture media indicates a role for autologous serum in enhancing phenotypic preservation of rabbit limbal stem cells in explant culture', *Cytotechnology*, 70: 687-700.

Gutierrez, S., and M. D. Boada. 2018. 'Neuropeptide-induced modulation of carcinogenesis in a metastatic breast cancer cell line (MDA-MB-231(LUC+))', *Cancer Cell Int*, 18: 216.

Han, M. L. K., E. Arteaga-Solis, J. Blenis, G. Bourjeily, D. J. Clegg, D. Demeo, J. Duffy, B. Gaston, N. M. Heller, A. Hemnes, E. P. Henske, R. Jain, T. Lahm, L. H. Lancaster, J. Lee, M. J. Legato, S. Mckee, R. Mehra, A. Morris, Y. S. Prakash, M. R. Stampfli, R. Gopal-Srivastava, A. D. Laposky, A. Punturieri, L. Reineck, X. Tigno, and J. Clayton. 2018. 'Female Sex and Gender in Lung/Sleep Health and Disease Increased Understanding of Basic Biological, Pathophysiological, and Behavioral Mechanisms Leading to Better Health for Female Patients with Lung Disease', *American Journal of Respiratory and Critical Care Medicine*, 198: 850-58.

Hartje, L. F., H. T. Bui, D. A. Andales, S. P. James, T. R. Huber, and C. D. Snow. 2018. 'Characterizing the Cytocompatibility of Various Cross-Linking Chemistries for the Production of Biostable Large-Pore Protein Crystal Materials', *ACS Biomater Sci Eng*, 4: 826-31.

Hartje, L. F., B. Munsky, T. W. Ni, C. J. Ackerson, and C. D. Snow. 2017. 'Adsorption-Coupled Diffusion of Gold Nanoclusters within a Large-Pore Protein Crystal Scaffold', *J Phys Chem B*, 121: 7652-59.

Held, H. D., C. Martin, and S. Uhlig. 1999. 'Characterization of airway and vascular responses in murine lungs', *Br J Pharmacol*, 126: 1191-9.

Henjakovic, M., K. Sewald, S. Switalla, D. Kaiser, M. Muller, T. Z. Veres, C. Martin, S. Uhlig, N. Krug, and A. Braun. 2008. 'Ex vivo testing of immune responses in precision-cut lung slices', *Toxicol Appl Pharmacol*, 231: 68-76.

Hong, Y., W. Ji, S. An, S. S. Han, S. J. Lee, and W. J. Kim. 2016. 'Sex differences of COPD phenotypes in nonsmoking patients', *International Journal of Chronic Obstructive Pulmonary Disease*, 11: 1657-62.

Hoppener, J. W., P. H. Steenbergh, R. J. Slebos, A. Visser, C. J. Lips, H. S. Jansz, J. M. Bechet, G. M. Lenoir, W. Born, S. Haller-Brem, and et al. 1987. 'Expression of the second calcitonin/calcitonin gene-related peptide gene in Ewing sarcoma cell lines', *J Clin Endocrinol Metab*, 64: 809-17.

Hussain, I., G. L. Y. Cher, M. A. Abid, and M. B. Abid. 2021. 'Role of Gut Microbiome in COVID-19: An Insight Into Pathogenesis and Therapeutic Potential', *Frontiers in Immunology*, 12.

Inam, Z., E. Felton, A. Burrell, H. Chaney, I. Sami, A. C. Koumbourlis, R. J. Freishtat, E. T. Zemanick, K. A. Crandall, and A. Hahn. 2022. 'Impact of Antibiotics on the Lung Microbiome and Lung Function in Children With Cystic Fibrosis 1 Year After Hospitalization for an Initial Pulmonary Exacerbation', *Open Forum Infect Dis*, 9: ofac466.

Jacobsen, H., and S. L. Klein. 2021. 'Sex Differences in Immunity to Viral Infections', *Frontiers in Immunology*, 12: 720952.

Jain, R., C. E. Barkauskas, N. Takeda, E. J. Bowie, H. Aghajanian, Q. Wang, A. Padmanabhan, L. J. Manderfield, M. Gupta, D. Li, L. Li, C. M. Trivedi, B. L. M.

Hogan, and J. A. Epstein. 2015. 'Plasticity of Hopx(+) type I alveolar cells to regenerate type II cells in the lung', *Nature Communications*, 6: 6727.

Janeway, C. A., Jr. 2001. 'How the immune system protects the host from infection', *Microbes Infect*, 3: 1167-71.

Jansing, N. L., J. McClendon, P. M. Henson, R. M. Tuder, D. M. Hyde, and R. L. Zemans. 2017. 'Unbiased Quantitation of Alveolar Type II to Alveolar Type I Cell Transdifferentiation during Repair after Lung Injury in Mice', *Am J Respir Cell Mol Biol*, 57: 519-26.

Jean, E. E., O. Good, J. M. I. Rico, H. L. Rossi, and D. R. Herbert. 2022. 'Neuroimmune regulatory networks of the airway mucosa in allergic inflammatory disease', *J Leukoc Biol*, 111: 209-21.

Jimenez-Valdes, R. J., U. I. Can, B. F. Niemeyer, and K. H. Benam. 2020. 'Where We Stand: Lung Organotypic Living Systems That Emulate Human-Relevant Host-Environment/Pathogen Interactions', *Front Bioeng Biotechnol*, 8: 989.

Jin, J. M., P. Bai, W. He, F. Wu, X. F. Liu, D. M. Han, S. Liu, and J. K. Yang. 2020. 'Gender Differences in Patients With COVID-19: Focus on Severity and Mortality', *Front Public Health*, 8: 152.

Kaczynska, K., D. Zajac, P. Wojciechowski, E. Kogut, and M. Szereda-Przestaszewska. 2018. 'Neuropeptides and breathing in health and disease', *Pulm Pharmacol Ther*, 48: 217-24.

Kapalczynska, M., T. Kolenda, W. Przybyla, M. Zajaczkowska, A. Teresiak, V. Filas, M. Ibbs, R. Blizniak, L. Luczewski, and K. Lamperska. 2018. '2D and 3D cell cultures

- a comparison of different types of cancer cell cultures', *Archives of Medical Science*, 14: 910-19.

Kaul, D., R. Rathnasinghe, M. Ferres, G. S. Tan, A. Barrera, B. E. Pickett, B. A. Methe, S. R. Das, I. Budnik, R. A. Halpin, D. Wentworth, M. Schmolke, I. Mena, R. A. Albrecht, I. Singh, K. E. Nelson, A. Garcia-Sastre, C. L. Dupont, and R. A. Medina. 2020. 'Microbiome disturbance and resilience dynamics of the upper respiratory tract during influenza A virus infection (vol 52, pg 631, 2020)', *Nature Communications*, 11.

Kautzky-Willer, A., M. Kaleta, S. D. Lindner, M. Leutner, S. Thurner, and P. Klimek. 2022. 'Sex Differences in Clinical Characteristics and Outcomes of Patients with SARS-CoV-2-Infection Admitted to Intensive Care Units in Austria', *Journal of Personalized Medicine*, 12.

Kawanami, Y., Y. Morimoto, H. Kim, T. Nakamura, K. Machida, T. Kido, E. Asonuma, K. Yatera, C. Yoshii, and M. Kido. 2009. 'Calcitonin gene-related peptide stimulates proliferation of alveolar epithelial cells', *Respir Res*, 10: 8.

Kee, Z., X. Kodji, and S. D. Brain. 2018. 'The Role of Calcitonin Gene Related Peptide (CGRP) in Neurogenic Vasodilation and Its Cardioprotective Effects', *Front Physiol*, 9: 1249.

Kiener, M., N. Roldan, C. Machahua, A. Sengupta, T. Geiser, O. T. Guenat, M. Funke-Chambour, N. Hobi, and M. Kruithof-de Julio. 2021. 'Human-Based Advanced in vitro Approaches to Investigate Lung Fibrosis and Pulmonary Effects of COVID-19', *Front Med (Lausanne)*, 8: 644678.

Klein, S. L., B. H. Bird, and G. E. Glass. 2001. 'Sex differences in immune responses and viral shedding following Seoul virus infection in Norway rats', *Am J Trop Med Hyg*, 65: 57-63.

Klein, S. L., and K. L. Flanagan. 2016. 'Sex differences in immune responses', *Nat Rev Immunol*, 16: 626-38.

Kokoszynska, M., N. D. Ubags, J. J. Bivona, S. Ventrone, L. F. Reed, A. E. Dixon, M. J. Wargo, M. E. Poynter, and B. T. Suratt. 2021. 'Storage conditions of high-fat diets affect pulmonary inflammation', *Physiological Reports*, 9.

Kummer, W., S. Wiegand, S. Akinci, A. H. Schinkel, J. Wess, H. Koepsell, R. V. Haberberger, and K. S. Lips. 2006. 'Role of acetylcholine and muscarinic receptors in serotonin-induced bronchoconstriction in the mouse', *J Mol Neurosci*, 30: 67-8.

Labiris, N. R., and M. B. Dolovich. 2003a. 'Pulmonary drug delivery. Part I: physiological factors affecting therapeutic effectiveness of aerosolized medications', *Br J Clin Pharmacol*, 56: 588-99.

———. 2003b. 'Pulmonary drug delivery. Part II: the role of inhalant delivery devices and drug formulations in therapeutic effectiveness of aerosolized medications', *Br J Clin Pharmacol*, 56: 600-12.

Lam, M., E. Lamanna, and J. E. Bourke. 2019. 'Regulation of Airway Smooth Muscle Contraction in Health and Disease', *Lung Inflammation in Health and Disease, Vol Ii*, 1124: 381-422.

Leiby, K. L., R. Ng, S. G. Campbell, and L. E. Niklason. 2022. 'Engineered Lung Tissues Prepared from Decellularized Lung Slices', *J Vis Exp*.

Levesque, B. M., R. J. Vosatka, and H. C. Nielsen. 2000. 'Dihydrotestosterone stimulates branching morphogenesis, cell proliferation, and programmed cell death in mouse embryonic lung explants', *Pediatr Res*, 47: 481-91.

Li, G., J. A. Cohen, C. Martines, S. Ram-Mohan, J. D. Brain, R. Krishnan, X. Ai, and Y. Bai. 2020. 'Preserving Airway Smooth Muscle Contraction in Precision-Cut Lung Slices', *Sci Rep*, 10: 6480.

Li, X., X. Cao, M. Guo, M. Xie, and X. Liu. 2020. 'Trends and risk factors of mortality and disability adjusted life years for chronic respiratory diseases from 1990 to 2017: systematic analysis for the Global Burden of Disease Study 2017', *BMJ*, 368: m234.

Liu, G., C. Betts, D. M. Cunoosamy, P. M. Aberg, J. J. Hornberg, K. B. Sivars, and T. S. Cohen. 2019. 'Use of precision cut lung slices as a translational model for the study of lung biology', *Respir Res*, 20: 162.

LoMauro, A., and A. Aliverti. 2018. 'Sex differences in respiratory function', *Breathe (Sheff)*, 14: 131-40.

Lopez, A. D., and C. D. Mathers. 2006. 'Measuring the global burden of disease and epidemiological transitions: 2002-2030', *Ann Trop Med Parasitol*, 100: 481-99.

Lopez, A. D., C. D. Mathers, M. Ezzati, D. T. Jamison, and C. J. L. Murray. 2006. 'Measuring the Global Burden of Disease and Risk Factors, 1990-2001.' in A. D. Lopez, C. D. Mathers, M. Ezzati, D. T. Jamison and C. J. L. Murray (eds.), *Global Burden of Disease and Risk Factors* (Washington (DC)

New York).

Lyons-Cohen, M. R., S. Y. Thomas, D. N. Cook, and H. Nakano. 2017. 'Precision-cut Mouse Lung Slices to Visualize Live Pulmonary Dendritic Cells', *J Vis Exp*.

Mathers, C. D., T. Boerma, and D. Ma Fat. 2009. 'Global and regional causes of death', *Br Med Bull*, 92: 7-32.

Mazaheri, T., R. Ranasinghe, W. Al-Hasani, J. Luxton, J. Kearney, A. Manning, G. K. Dimitriadis, T. Mare, and R. P. Vincent. 2022. 'A cytokine panel and procalcitonin in COVID-19, a comparison between intensive care and non-intensive care patients', *PLoS One*, 17: e0266652.

McNicholas, B. A., F. Madotto, T. Pham, E. Rezoagli, C. H. Masterson, S. Horie, G. Bellani, L. Brochard, J. G. Laffey, LUNG Safe Investigators, and ESICM Trials Grp. 2019. 'Demographics, management and outcome of females and males with acute respiratory distress syndrome in the LUNG SAFE prospective cohort study', *European Respiratory Journal*, 54.

Melssen, M. M., G. R. Petroni, K. A. Chianese-Bullock, N. A. Wages, W. W. Grosh, N. Varhegyi, M. E. Smolkin, K. T. Smith, N. V. Galeassi, D. H. Deacon, E. M. Gaughan, and C. L. Slingluff, Jr. 2019. 'A multipeptide vaccine plus toll-like receptor agonists LPS or polyICLC in combination with incomplete Freund's adjuvant in melanoma patients', *J Immunother Cancer*, 7: 163.

Mou, H., Y. Yang, M. A. Riehs, J. Barrios, M. Shivaraju, A. L. Haber, D. T. Montoro, K. Gilmore, E. A. Haas, B. Paunovic, J. Rajagopal, S. O. Vargas, R. L. Haynes, A. Fine, W. V. Cardoso, and X. Ai. 2021. 'Airway basal stem cells generate distinct subpopulations of PNECs', *Cell Rep*, 35: 109011.

Nagashima, H., T. Mahlakoiv, H. Y. Shih, F. P. Davis, F. Meylan, Y. Huang, O. J. Harrison, C. Yao, Y. Mikami, J. F. Urban, Jr., K. M. Caron, Y. Belkaid, Y. Kanno, D. Artis, and J. J. O'Shea. 2019. 'Neuropeptide CGRP Limits Group 2 Innate Lymphoid Cell Responses and Constrains Type 2 Inflammation', *Immunity*, 51: 682-95 e6.

Newman, S. P. 2017. 'Drug delivery to the lungs: challenges and opportunities', *Ther Deliv*, 8: 647-61.

Niemeyer, B. F., P. Zhao, R. M. Tuder, and K. H. Benam. 2018. 'Advanced Microengineered Lung Models for Translational Drug Discovery', *SLAS Discov*, 23: 777-89.

Noguchi, M., K. T. Furukawa, and M. Morimoto. 2020. 'Pulmonary neuroendocrine cells: physiology, tissue homeostasis and disease', *Dis Model Mech*, 13.

Ollila, J., and M. Vihinen. 2005. 'B cells', *Int J Biochem Cell Biol*, 37: 518-23.

Oslund, K. L., D. M. Hyde, L. F. Putney, M. F. Alfaro, W. F. Walby, N. K. Tyler, and E. S. Schelegle. 2009. 'Activation of calcitonin gene-related peptide receptor during ozone inhalation contributes to airway epithelial injury and repair', *Toxicol Pathol*, 37: 805-13.

Ostrovskaya, A., C. Hick, D. S. Hutchinson, B. W. Stringer, P. J. Wookey, D. Wootten, P. M. Sexton, and S. G. B. Furness. 2019. 'Expression and activity of the calcitonin receptor family in a sample of primary human high-grade gliomas', *BMC Cancer*, 19: 157.

Ouadah, Y., E. R. Rojas, D. P. Riordan, S. Capostagno, C. S. Kuo, and M. A. Krasnow. 2019. 'Rare Pulmonary Neuroendocrine Cells Are Stem Cells Regulated by Rb, p53, and Notch', *Cell*, 179: 403-16 e23.

Patel, V., K. Amin, D. Allen, L. Ukishima, A. Wahab, C. Grodi, and H. Behrsing. 2021. 'Comparison of Long-term Human Precision-cut Lung Slice Culture Methodology and Response to Challenge: An Argument for Standardisation', *Altern Lab Anim*, 49: 209-22.

Patlin, Brielle. 2022. "Calcitonin Gene Related Peptide (CGRP) Modulates B cells in the Lung Neuroimmune Axis Abstract." In, edited by Stuart Tobet. Society for Neuroscience Conference.

Pearson, R. M. 1986. 'In-vitro techniques: can they replace animal testing?', *Hum Reprod*, 1: 559-60.

Preuss, E. B., S. Schubert, C. Werlein, H. Stark, P. Braubach, A. Hofer, E. K. J. Plucinski, H. R. Shah, R. Geffers, K. Sewald, A. Braun, D. D. Jonigk, and M. P. Kuhnel. 2022. 'The Challenge of Long-Term Cultivation of Human Precision-Cut Lung Slices', *Am J Pathol*, 192: 239-53.

Ptasinski, V. A., J. Stegmayr, M. G. Belvisi, D. E. Wagner, and L. A. Murray. 2021. 'Targeting Alveolar Repair in Idiopathic Pulmonary Fibrosis', *Am J Respir Cell Mol Biol*, 65: 347-65.

Rashid, A., and A. Manghi. 2022. 'Calcitonin Gene-Related Peptide Receptor.' in, *StatPearls* (Treasure Island (FL)).

Ray, J. C., P. Allen, A. Bacsi, J. J. Bosco, L. Chen, M. Eller, H. Kua, L. L. Lim, M. S. Matharu, M. Monif, M. Ruttledge, R. J. Stark, and E. J. Hutton. 2021.

'Inflammatory complications of CGRP monoclonal antibodies: a case series', *J Headache Pain*, 22: 121.

Regal, J. F., and D. E. Johnson. 1983. 'Indomethacin alters the effects of substance-P and VIP on isolated airway smooth muscle', *Peptides*, 4: 581-4.

Rello, J., I. Bello, R. de Vicente, A. Hermira Anchuelo, M. A. Ballesteros, R. Iranzo, L. Rellan, J. Riera, J. C. Robles, and Empret Study investigators. 2017. 'Risk Factors for Mortality in 272 Patients With Lung Transplant: A Multicenter Analysis of 7 Intensive Care Units', *Arch Bronconeumol*, 53: 421-26.

Rosenblum, D. A., M. V. Volpe, C. E. L. Dammann, Y. S. Lo, J. F. Thompson, and H. C. Nielsen. 1998. 'Expression and activity of epidermal growth factor receptor in late fetal rat lung is cell- and sex-specific', *Experimental Cell Research*, 239: 69-81.

Rosmark, O., A. Ibanez-Fonseca, J. Thorsson, G. Dellgren, O. Hallgren, A. K. Larsson Callerfelt, L. Elowsson, and G. Westergren-Thorsson. 2022. 'A tunable physiomimetic stretch system evaluated with precision cut lung slices and recellularized human lung scaffolds', *Front Bioeng Biotechnol*, 10: 995460.

Ruigrok, M. J. R., J. Tomar, H. W. Frijlink, B. N. Melgert, W. L. J. Hinrichs, and P. Olinga. 2019. 'The effects of oxygen concentration on cell death, anti-oxidant transcription, acute inflammation, and cell proliferation in precision-cut lung slices', *Sci Rep*, 9: 16239.

Russell, F. A., R. King, S. J. Smillie, X. Kodji, and S. D. Brain. 2014. 'Calcitonin Gene-Related Peptide: Physiology and Pathophysiology', *Physiological Reviews*, 94: 1099-142.

Sauer, U. G., S. Vogel, A. Aumann, A. Hess, S. N. Kolle, L. Ma-Hock, W. Wohlleben, M. Dammann, V. Strauss, S. Treumann, S. Groters, K. Wiench, B. van Ravenzwaay, and R. Landsiedel. 2014. 'Applicability of rat precision-cut lung slices in evaluating nanomaterial cytotoxicity, apoptosis, oxidative stress, and inflammation', *Toxicol Appl Pharmacol*, 276: 1-20.

Sauler, M., I. S. Bazan, and P. J. Lee. 2019. 'Cell Death in the Lung: The Apoptosis-Necroptosis Axis', *Annu Rev Physiol*, 81: 375-402.

Schleputz, M., A. D. Rieg, S. Seehase, J. Spillner, A. Perez-Bouza, T. Braunschweig, T. Schroeder, M. Bernau, V. Lambermont, C. Schlumbohm, K. Sewald, R. Autschbach, A. Braun, B. W. Kramer, S. Uhlig, and C. Martin. 2012. 'Neurally mediated airway constriction in human and other species: a comparative study using precision-cut lung slices (PCLS)', *PLoS One*, 7: e47344.

Schuster, D., C. Laggner, and T. Langer. 2005. 'Why drugs fail--a study on side effects in new chemical entities', *Curr Pharm Des*, 11: 3545-59.

Schwerdtfeger, L. A., N. J. Nealon, E. P. Ryan, and S. A. Tobet. 2019. 'Human colon function ex vivo: Dependence on oxygen and sensitivity to antibiotic', *PLoS One*, 14: e0217170.

Schwerdtfeger, L. A., E. P. Ryan, and S. A. Tobet. 2016. 'An organotypic slice model for ex vivo study of neural, immune, and microbial interactions of mouse intestine', *Am J Physiol Gastrointest Liver Physiol*, 310: G240-8.

Shivaraju, M., U. K. Chitta, R. M. H. Grange, I. H. Jain, D. Capen, L. Liao, J. Xu, F. Ichinose, W. M. Zapol, V. K. Mootha, and J. Rajagopal. 2021. 'Airway stem cells

sense hypoxia and differentiate into protective solitary neuroendocrine cells', *Science*, 371: 52-57.

Singh, Y., G. Gupta, B. Shrivastava, R. Dahiya, J. Tiwari, M. Ashwathanarayana, R. K. Sharma, M. Agrawal, A. Mishra, and K. Dua. 2017. 'Calcitonin gene-related peptide (CGRP): A novel target for Alzheimer's disease', *CNS Neurosci Ther*, 23: 457-61.

Smith, L. K., I. W. Babcock, L. S. Minamide, A. E. Shaw, J. R. Bamburg, and T. B. Kuhn. 2021. 'Direct interaction of HIV gp120 with neuronal CXCR4 and CCR5 receptors induces cofilin-actin rod pathology via a cellular prion protein- and NOX-dependent mechanism', *PLoS One*, 16.

Song, H., E. Yao, C. Lin, R. Gacayan, M. H. Chen, and P. T. Chuang. 2012. 'Functional characterization of pulmonary neuroendocrine cells in lung development, injury, and tumorigenesis', *Proc Natl Acad Sci U S A*, 109: 17531-6.

Sponchiado, M., Y. Liao, K. R. Atanasova, E. N. Collins, V. A. Schurmann, L. Bravo, and L. Reznikov. 2021. 'Overexpression of Substance P in Pig Airways Increases MUC5AC Through a NF-kB Pathway', *American Journal of Respiratory and Critical Care Medicine*, 203.

Springer, J., and A. Fischer. 2003. 'Substance P-induced pulmonary vascular remodelling in precision cut lung slices', *European Respiratory Journal*, 22: 596-601.

Stout, A. J., A. B. Mirliani, M. L. Rittenberg, M. Shub, E. C. White, J. S. K. Yuen, Jr., and D. L. Kaplan. 2022. 'Simple and effective serum-free medium for sustained expansion of bovine satellite cells for cell cultured meat', *Commun Biol*, 5: 466.

Sui, P., D. L. Wiesner, J. Xu, Y. Zhang, J. Lee, S. Van Dyken, A. Lashua, C. Yu, B. S. Klein, R. M. Locksley, G. Deutsch, and X. Sun. 2018. 'Pulmonary neuroendocrine cells amplify allergic asthma responses', *Science*, 360.

Tejpal, A., E. Gianos, J. Cerise, J. S. Hirsch, S. Rosen, N. Kohn, M. Lesser, C. Weinberg, D. Majure, S. K. Satapathy, D. Bernstein, M. A. Barish, A. C. Spyropoulos, and R. M. Brown. 2021. 'Sex-Based Differences in COVID-19 Outcomes', *Journal of Womens Health*, 30: 492-501.

Thabut, G., and H. Mal. 2017. 'Outcomes after lung transplantation', *J Thorac Dis*, 9: 2684-91.

Tiwari, G., R. Tiwari, B. Sriwastawa, L. Bhati, S. Pandey, P. Pandey, and S. K. Bannerjee. 2012. 'Drug delivery systems: An updated review', *Int J Pharm Investig*, 2: 2-11.

Tobet, S. A., H. J. Walker, M. L. Seney, and K. W. Yu. 2003. 'Viewing cell movements in the developing neuroendocrine brain', *Integr Comp Biol*, 43: 794-801.

Townsend, E. A., V. M. Miller, and Y. S. Prakash. 2012. 'Sex Differences and Sex Steroids in Lung Health and Disease', *Endocrine Reviews*, 33: 1-47.

Trigueros, J. A., J. A. Riesco, B. Alcazar-Navarrete, A. Campuzano, and J. Perez. 2019. 'Clinical Features Of Women With COPD: Sex Differences In A Cross-Sectional Study In Spain ("The ESPIRAL-ES Study")', *International Journal of Chronic Obstructive Pulmonary Disease*, 14: 2469-78.

Uhl, F. E., S. Vierkotten, D. E. Wagner, G. Burgstaller, R. Costa, I. Koch, M. Lindner, S. Meiners, O. Eickelberg, and M. Konigshoff. 2015. 'Preclinical validation and

imaging of Wnt-induced repair in human 3D lung tissue cultures', *European Respiratory Journal*, 46: 1150-66.

Ursin, R. L., and S. L. Klein. 2021. 'Sex Differences in Respiratory Viral Pathogenesis and Treatments', *Annu Rev Virol*, 8: 393-414.

Usta, S. N., C. D. Scharer, J. Xu, T. K. Frey, and R. J. Nash. 2014. 'Chemically defined serum-free and xeno-free media for multiple cell lineages', *Ann Transl Med*, 2: 97.

Valavanidis, A., T. Vlachogianni, K. Fiotakis, and S. Loridas. 2013. 'Pulmonary oxidative stress, inflammation and cancer: respirable particulate matter, fibrous dusts and ozone as major causes of lung carcinogenesis through reactive oxygen species mechanisms', *Int J Environ Res Public Health*, 10: 3886-907.

van den Berg, M. P. M., S. Nijboer-Brinksma, I. S. T. Bos, M. van den Berge, D. Lamb, M. van Faassen, I. P. Kema, R. Gosens, and L. E. M. Kistemaker. 2021. 'The novel TRPA1 antagonist BI01305834 inhibits ovalbumin-induced bronchoconstriction in guinea pigs', *Respir Res*, 22: 48.

Van Norman, G. A. 2019. 'Limitations of Animal Studies for Predicting Toxicity in Clinical Trials: Is it Time to Rethink Our Current Approach?', *JACC Basic Transl Sci*, 4: 845-54.

Vandamme, T. F. 2014. 'Use of rodents as models of human diseases', *J Pharm Bioallied Sci*, 6: 2-9.

Venkataraman, C., G. Shankar, G. Sen, and S. Bondada. 1999. 'Bacterial lipopolysaccharide induced B cell activation is mediated via a

phosphatidylinositol 3-kinase dependent signaling pathway', *Immunol Lett*, 69: 233-8.

Viana, F., C. M. O'Kane, and G. N. Schroeder. 2022. 'Precision-cut lung slices: A powerful ex vivo model to investigate respiratory infectious diseases', *Mol Microbiol*, 117: 578-88.

Voedisch, S., S. Rochlitzer, T. Z. Veres, E. Spies, and A. Braun. 2012. 'Neuropeptides control the dynamic behavior of airway mucosal dendritic cells', *PLoS One*, 7: e45951.

vom Steeg, L. G., S. Dhakal, Y. A. Woldetsadik, H. S. Park, K. R. Mulka, E. C. Reilly, D. J. Topham, and S. L. Klein. 2020. 'Androgen receptor signaling in the lungs mitigates inflammation and improves the outcome of influenza in mice', *Plos Pathogens*, 16.

Wallrapp, A., P. R. Burkett, S. J. Riesenfeld, S. J. Kim, E. Christian, R. E. Abdulnour, P. I. Thakore, A. Schnell, C. Lambden, R. H. Herbst, P. Khan, K. Tsujikawa, R. J. Xavier, I. M. Chiu, B. D. Levy, A. Regev, and V. K. Kuchroo. 2019. 'Calcitonin Gene-Related Peptide Negatively Regulates Alarmin-Driven Type 2 Innate Lymphoid Cell Responses', *Immunity*, 51: 709-23 e6.

Wang, Y., Z. Tang, H. Huang, J. Li, Z. Wang, Y. Yu, C. Zhang, J. Li, H. Dai, F. Wang, T. Cai, and N. Tang. 2018. 'Pulmonary alveolar type I cell population consists of two distinct subtypes that differ in cell fate', *Proc Natl Acad Sci U S A*, 115: 2407-12.

Williams, P. T. 2014. 'Dose-response relationship between exercise and respiratory disease mortality', *Med Sci Sports Exerc*, 46: 711-7.

Wu, H., Y. Zhou, Y. Wang, L. Tong, F. Wang, S. Song, L. Xu, B. Liu, H. Yan, and Z. Sun. 2021. 'Current State and Future Directions of Intranasal Delivery Route for Central Nervous System Disorders: A Scientometric and Visualization Analysis', *Front Pharmacol*, 12: 717192.

Xu, H., L. N. Liew, I. C. Kuo, C. H. Huang, D. L. Goh, and K. Y. Chua. 2008. 'The modulatory effects of lipopolysaccharide-stimulated B cells on differential T-cell polarization', *Immunology*, 125: 218-28.

Xu, J., J. Tao, and J. Wang. 2020. 'Design and Application in Delivery System of Intranasal Antidepressants', *Front Bioeng Biotechnol*, 8: 626882.

Ying, X., X. Qi, Y. Yin, H. Wang, H. Zhang, H. Jiang, L. Yang, and J. Wu. 2022. 'Allergens sensitization among children with allergic diseases in Shanghai, China: age and sex difference', *Respir Res*, 23: 95.

Zhang, P., F. Wang, J. Hu, and R. Sorrentino. 2013. 'Exploring the relationship between drug side-effects and therapeutic indications', *AMIA Annu Symp Proc*, 2013: 1568-77.

Zhang, Y. B., D. Xu, L. Bai, Y. M. Zhou, H. Zhang, and Y. L. Cui. 2022. 'A Review of Non-Invasive Drug Delivery through Respiratory Routes', *Pharmaceutics*, 14.

Zhang, Y., C. Lin, X. Wang, and T. Ji. 2020. 'Calcitonin gene-related peptide: A promising bridge between cancer development and cancer-associated pain in oral squamous cell carcinoma', *Oncol Lett*, 20: 253.

Zhou, Y., M. Zhang, G. Y. Sun, Y. P. Liu, W. Z. Ran, L. Peng, and C. X. Guan. 2013. 'Calcitonin gene-related peptide promotes the wound healing of human bronchial epithelial cells via PKC and MAPK pathways', *Regul Pept*, 184: 22-9.

Appendix 1/Supplemental Figures

At 24 and 72 h, the sizes of B cells in PCLS from females were significantly larger than the sizes of B cells in PCLS from males. Cells were an average of 11% larger (45 μm^2) in female slices compared to (40μm^2) males (Figure S4h; P = 0.037). There were no significant changes in the number of $CD19^+$ B cells counted at 24-, 72-, and 120- h ex vivo (P = 0.55). The number of B-cells in slices from females (51 +/- 0.21) was not notably different compared to the number in slices from males (54+/- 0.35). in controls at 24-, 72-, and 120- h ex vivo (Figure S4g; P < 0.22). Representative images of B cell clusters at 24- (Figure S4a, d) 72- (Figure S4b, e), and 120- h (Figure S4c, f) in male (Figure S4d-f) and female (Figure S4a-c) are shown. When compared in size, the size of male (Figure S4d-f) and female (Figure S4a-c) B cells area did not significantly change when measured at 24-, 72-, and 120- h ex vivo P =.97, P=0.36,).

There was no change in area of CGRP fibers measured at 24-, 72-, and 120-h *ex vivo* (P=0.86) and female slices did not exhibit a significant difference in CGRP area per ROI compared to male slices (Figure S3h; P < 0.9; F (4, 27)). No significant difference between male and female CGRP fiber area per ROI (Figure S3g) as shown in male (Figure S5a-c) and female (Figure S5d-f). Compared to total area of CGRP fibers in a male slice, area of female fibers is significantly lower at 24- (P<0.0001) 72-h (P=0.012) and 120-h (Figure S5h; P=0.0045). There was no change in total area per slice (P=0.76) or area per ROI (P=0.82) of Peripherin-ir fibers measured at 24-, 72-, and 120-h *ex vivo*. Female slices did not exhibit a difference (Figure S6g) in fiber area (Figure S6d-f) compared to male slices figure (Figure S6a-c; P=0.26; F (1, 28)).

There was no significant change in size (Figure S7h; P = 0.67) or number (Figure S59g; P = 0.84) of SPC granules seen across five days *ex vivo* seen in males (Figure S7a-c) or females (Figure S7d-f). Male granules were significantly larger than female granules at 24 h (Figure S7a/d; P = 0.011) and 120-h (Figure S75c/f; P = 0.007 and trended towards being larger at 72-h *ex vivo* (Figure S7b/e; P = 0.088).

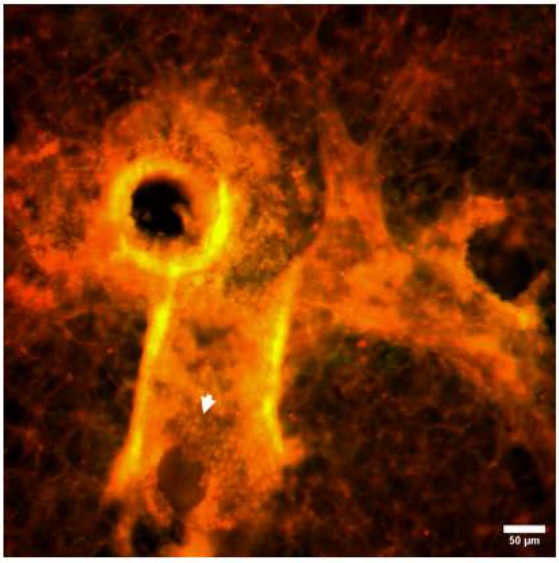

Figure S1: Tissue slices demonstrated the ability to incorporate exogenous carbohydrate (GalNaz) into mucopolysaccharides suggesting mucus was being produced. Scale bars are 50µm.

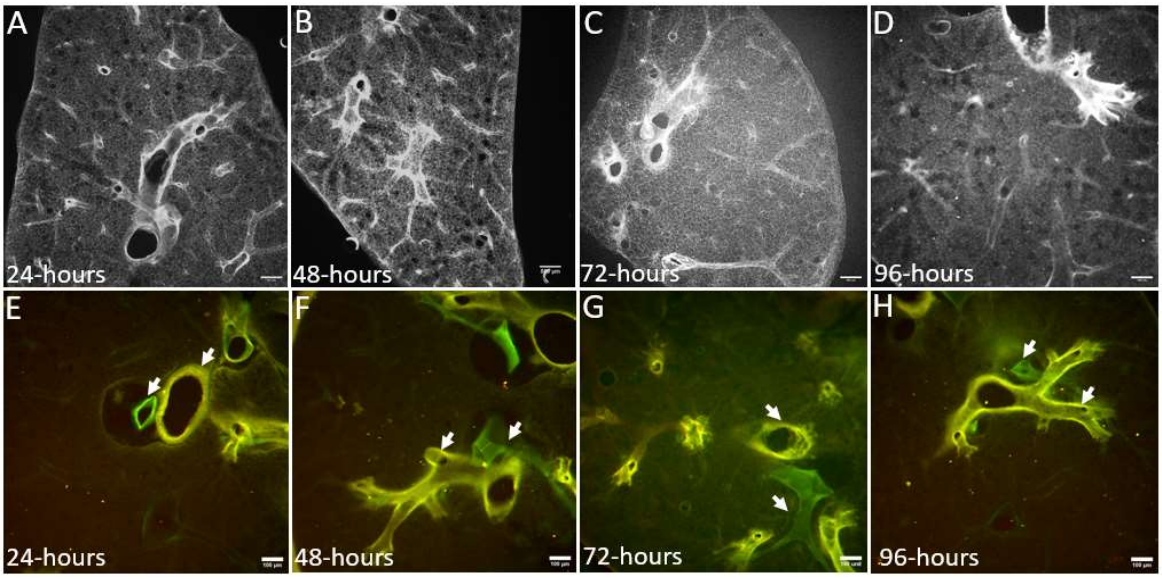

Figure S2: Morphology of lung slices from C57BL6/J Thy1-YFP transgenic mice across 96 h ex vivo. Low magnification images A-D excited with at 488nm can be compared with higher magnification images of Fluorescein isothiocyanate (FITC) perfused tissue to display airways (yellow) and blood vessels (green) in red (550 excitation) and green (488nm excitation) overlayed images. Scale bars are 100µm.

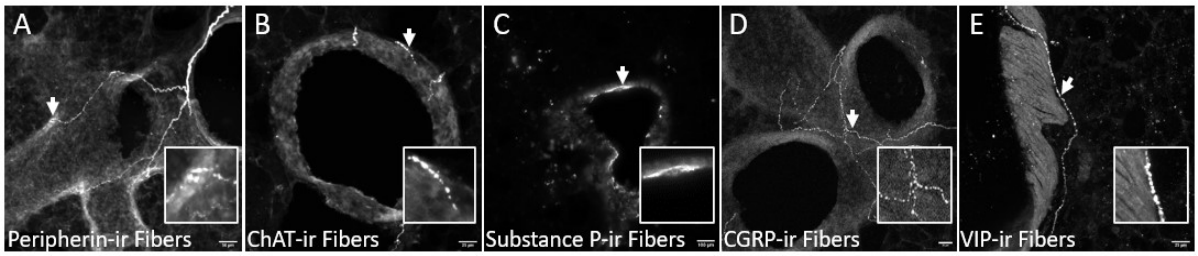

Figure S3: Immunohistochemical labeling of neuronal fibers in the lung. A. Peripherin is a peripheral neuronal intermediate filament protein that serves as a comprehensive marker for neuronal fibers in the lung; immunoreactive (ir) cell bodies were seen in some images. B. Choline acetyltransferase (ChAT)-ir fibers are a marker for cholinergic fibers likely of vagal origin. C. Substance P-ir fibers. D. CGRP-ir fibers and ir-CGRP was also found in pulmonary neuroendocrine cells and neuroendocrine bodies. E. Vasoactive intestinal peptide (VIP). Scale bars are 100μm.

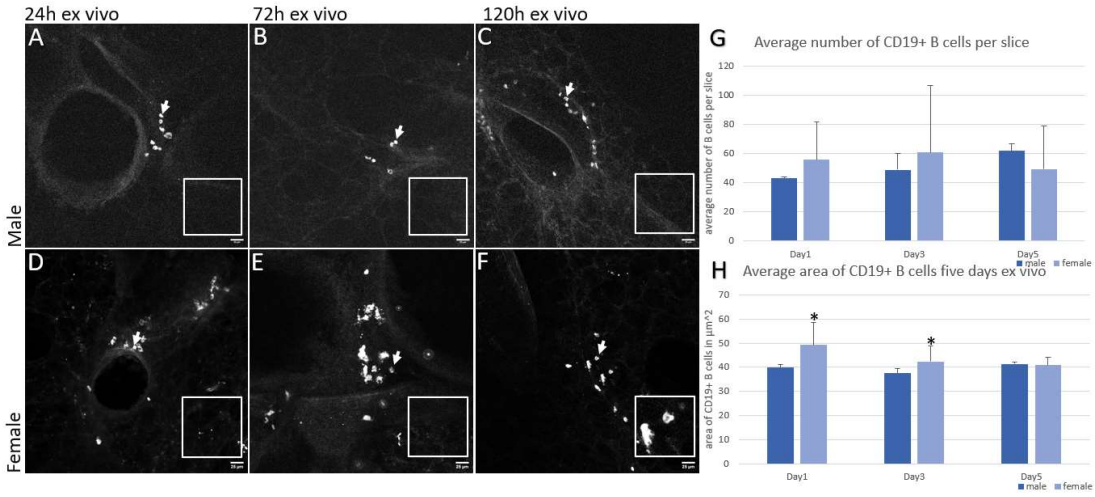

Figure S4: There were no significant differences in number of sizes of B cells between sexes over five days ex vivo. There were no significant changes in size or number of B cells in slices from males or females B cells from 24 – 120 h ex vivo. Areas of B cells in slices from females were greater than the areas of B cells in slices from males. * Indicates significance between males and females. A-C. Lung slices from males containing B cells from 24-120h ex vivo. D-F. Lung slices from females showing B cells from 24-120h ex vivo. Scale bars are 25μm.

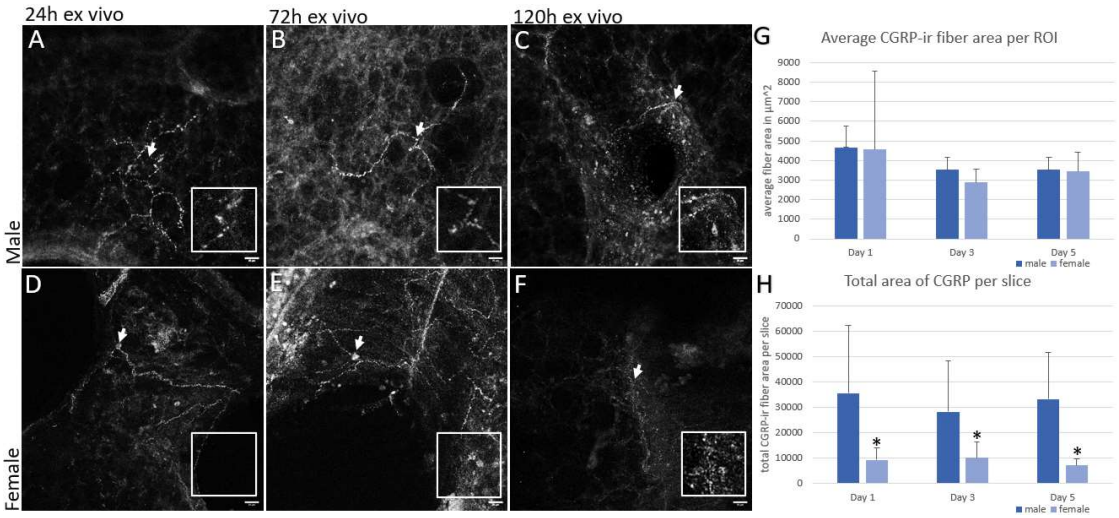

Figure S5: There are more CGRP-ir fibers per slice in males than females. There is no significant change in CGRP-ir fibers from 24 – 120 h ex vivo. * Indicates significance between males and females. A-C. Male lung slices labeled for CGRP showing CGRP-ir fibers and pulmonary neuroendocrine cells. D-F. Female lung slices showing B cells from 24 – 120 h ex vivo. Scale bars are 25µm.

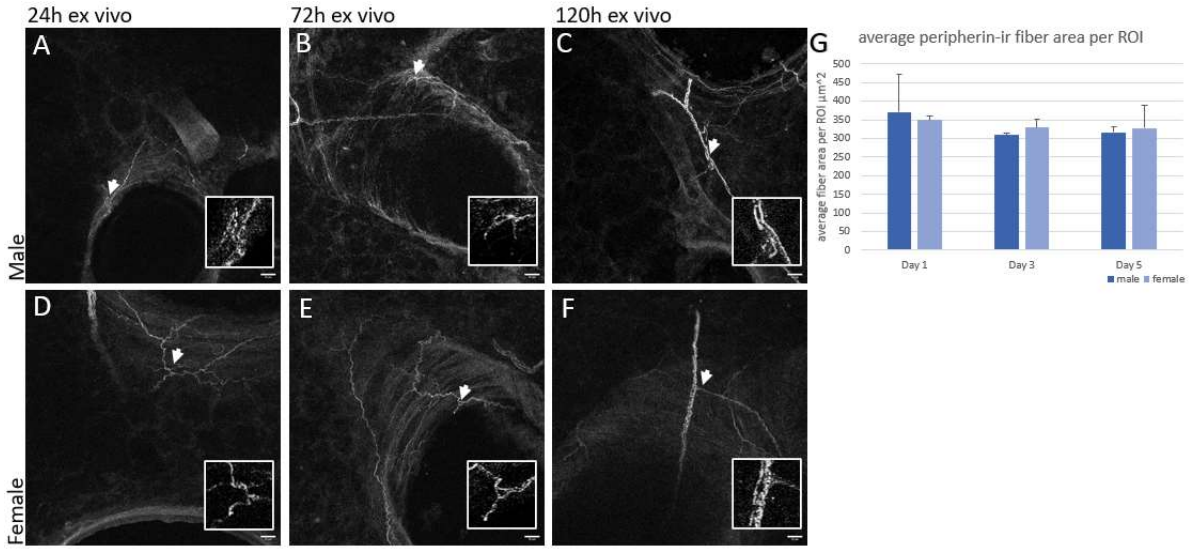

Figure S6: Average area of immunoreactive (ir) peripherin fibers did not change across 24 – 120 h in slices from males or females. There was no sex difference for average fiber area. A-C. Lung slices from males demonstrating ir-peripherin fibers and cell bodies. D-F Lung slices from females demonstrating ir-peripherin fibers and cell bodies. Scale bars are 25µm.

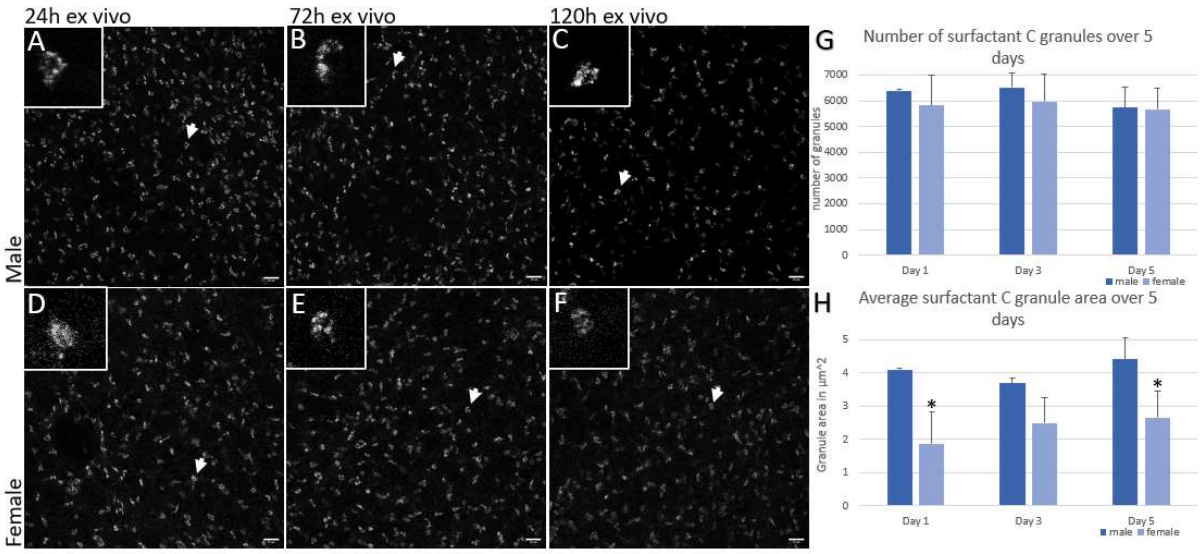

Figure S7: Number and area of immunoreactive (ir) SPC labeled granules produced by alveolar type 2 cells did not change over five days *ex vivo*. ir-SPC granules in slices from females were smaller significantly smaller at 24 h and 120 h and trends toward being smaller at 72 h. * indicates significance between data from slices originating from males and females. A-C. Male lung slices across 24-120 h ex vivo showing ir-SPC. D-F Lung slices from females across 24 – 120 h ex vivo showing ir-SPC. Scale bars are 25µm.

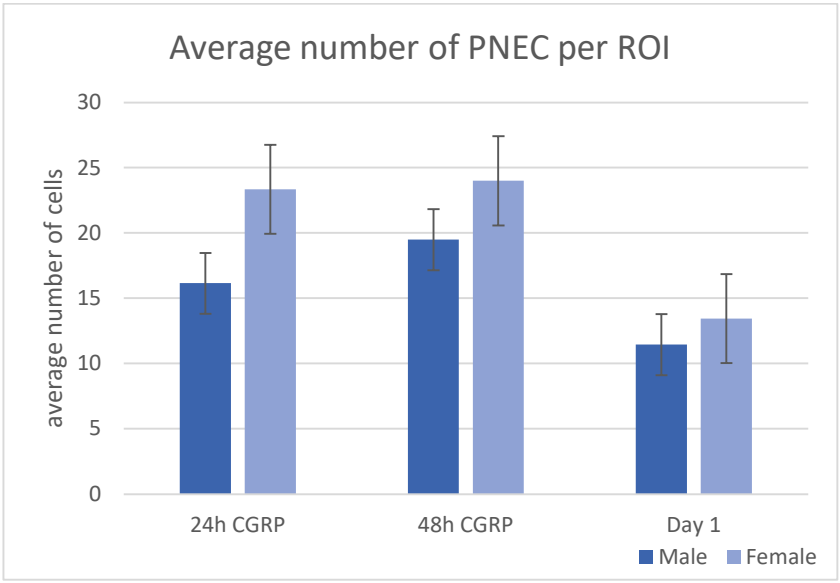

Figure S8: There was no change in the number of pulmonary neuroendocrine cells (PNECs) with 24 or 48 h exposure to exogenous CGRP compared to vehicle. No sex differences were observed.